Scientific Research Publishing

Open Journal of Geology, 2025, 15(12), 1061-1091
https://www.scirp.org/journal/ojg
ISSN Online: 2161-7589
ISSN Print: 2161-7570

Petrographic and Geochemical Characterization of the Fianga Granitoids (Mayo Kebbi) in the Pan-African Range of Central Africa in Chad: Geodynamic Implication

Moussa Ngarena Klamadji[1*], Diondoh Mbaguedje[2], Nenadji Félix Djerossem[3], Ronang Gustave Baïssemia[1], Djoum Temoua[1]

[1]Department of Mining and Geological Engineering, Faculty of Life and Earth Sciences, Pala University, Pala, Chad
[2]Department of Geological, Faculty of Life and Earth Sciences, Adam Barka University of Abeché, Abeche, Chad
[3]Department of Mining, New and Renewable Energies, National Higher Institute of the Sahara and Sahel, Iriba, Chad
Email: *klamadjimoussa@yahoo.fr

How to cite this paper: Klamadji, M.N., Mbaguedje, D., Djerossem, N.F., Baïssemia, R.G. and Temoua, D. (2025) Petrographic and Geochemical Characterization of the Fianga Granitoids (Mayo Kebbi) in the Pan-African Range of Central Africa in Chad: Geodynamic Implication. *Open Journal of Geology*, **15**, 1061-1091.
https://doi.org/10.4236/ojg.2025.1512055

Received: October 11, 2025
Accepted: December 23, 2025
Published: December 26, 2025

Abstract

The Fianga Massif belongs to the Pan-African Range of Central Africa in Chad. The Fianga Massif belongs to the Chadian sector of the Pan-African Range of Central Africa. The Fianga area has not been the subject of a detailed geological study. Many gaps remain in terms of the petrography and geochemistry of the massif. The Fianga Massif is composed of small, elongated NW-SE plutons. It consists of granitoids (granodiorites, hornblende and biotite granites, biotite granites and biotite microgranites) intruding into metamorphic rocks (quartz chlorite schists and massive amphibolites). These granitoids contain enclaves of metamorphic rocks and are cut by aplite and pegmatite veins. Geochemistry demonstrates that the Fianga granitoids are highly potassic and peraluminous. These studied rocks originate from a single magmatic source that evolved and differentiated by fractional crystallization in a magmatic reservoir. REE profiles show weakly enriched REEs (LaN/YbN = 0.69 - 40.29) while heavy REEs show a nearly flat profile (DyN/YbN = 0.52 - 1.13), and the La/Sm and Sm/Yb ratios led to the proposal that the Fianga rocks were derived from the partial melting of a mantle source enriched in spinel-garnet lherzolite. The partial melting of this mantle source is linked to large-scale movements along the Central Cameroon or Adamawa-Yadé shear zone and the Tchollire-Banyo shear zone, which controlled the emplacement of the pluton in the study area during the Pan-African period. This partial melting would be the origin of the emplacement of the granitoids of the Fianga massif. The high La/Nb (0.30 - 8.66) and low La/Ba (0.012 - 0.36) ratios of these gran-

itoids are consistent with their origin by partial melting of the subcontinental lithospheric mantle modified by subduction. Pink granites (A/CNK = 0.91 - 0.96), pink microgranites (A/CNK = 0.98 - 0.07), syenites (A/CNK = 0.02), and granodiorites (A/CNK = 0.94 - 1.40) are metaluminous to peraluminous. The data suggest emplacement of this Fianga pluton in a subduction zone. The granitoids occur in the domains of volcanic arc granitoids and syn-collisional granites.

Keywords

Granitoids, Calc-Alkaline, Fianga Massif, Mayo-Kebbi, Pan-African Range

1. Introduction

The Pan-African Range of Central Africa (CPAC), identified in the early 1960s, is a vast geological complex located north of the Congo Craton [1]. It extends from the Central African Republic (CAR) to eastern Nigeria via Chad and Cameroon, and continues across the Atlantic in the Borborema Province in northeastern Brazil ([1] [2]; **Figure 1**). This chain corresponds to an orogen that formed between 700 and 500 Ma. In Chad, the identified Precambrian formations are distributed between the Tibesti massifs in the north, Ouaddaï in the east, Yadé or Baïbokoum in the south, Mayo Kebbi in the southwest and Guéra in the center. These formations are part of the Pan-African mobile zone [1] [3]-[6]. Granitoids, being a major component of the continental crust, appear to be extremely common in collisional belts, particularly in shear zones [7] [8]. They are intrinsically associated with the dynamics of mountain ranges and record deformation structures during their emplacement. It is through shear movements in the lithosphere that magmas in general are injected to lead to the complete formation of plutons.

The Fianga region, located on the peneplained surface of Paleo-Chadian formations [16], where the granitoids of the Fianga massif outcrop, is a geologically poorly known area that has been little studied in detail. This area has not been the subject of a detailed geological study. Many gaps remain in the petrography and geochemistry of the massif. There are many gaps in the petrography and geochemistry of the Fianga massif. Consequently, major questions remain about its petrogenesis and the geodynamic context of its formation. However, the Léré (SSW) and Pala (SW) regions which border it have better studied geological formations (magmatic, metamorphic and sedimentary) [3]-[5] [17]-[19]. What is the contribution of the geology of the Fianga massif to the geological knowledge of the Pan-African Range of Central Africa?

2. Geological Context

In Africa, there are several Pan-African belts, including those of Central Africa, or the Central African "mobile zone" [1] [20]. It corresponds to an orogenic megabelt elongated in an E-W direction, over 5000 km long and 300 km wide,

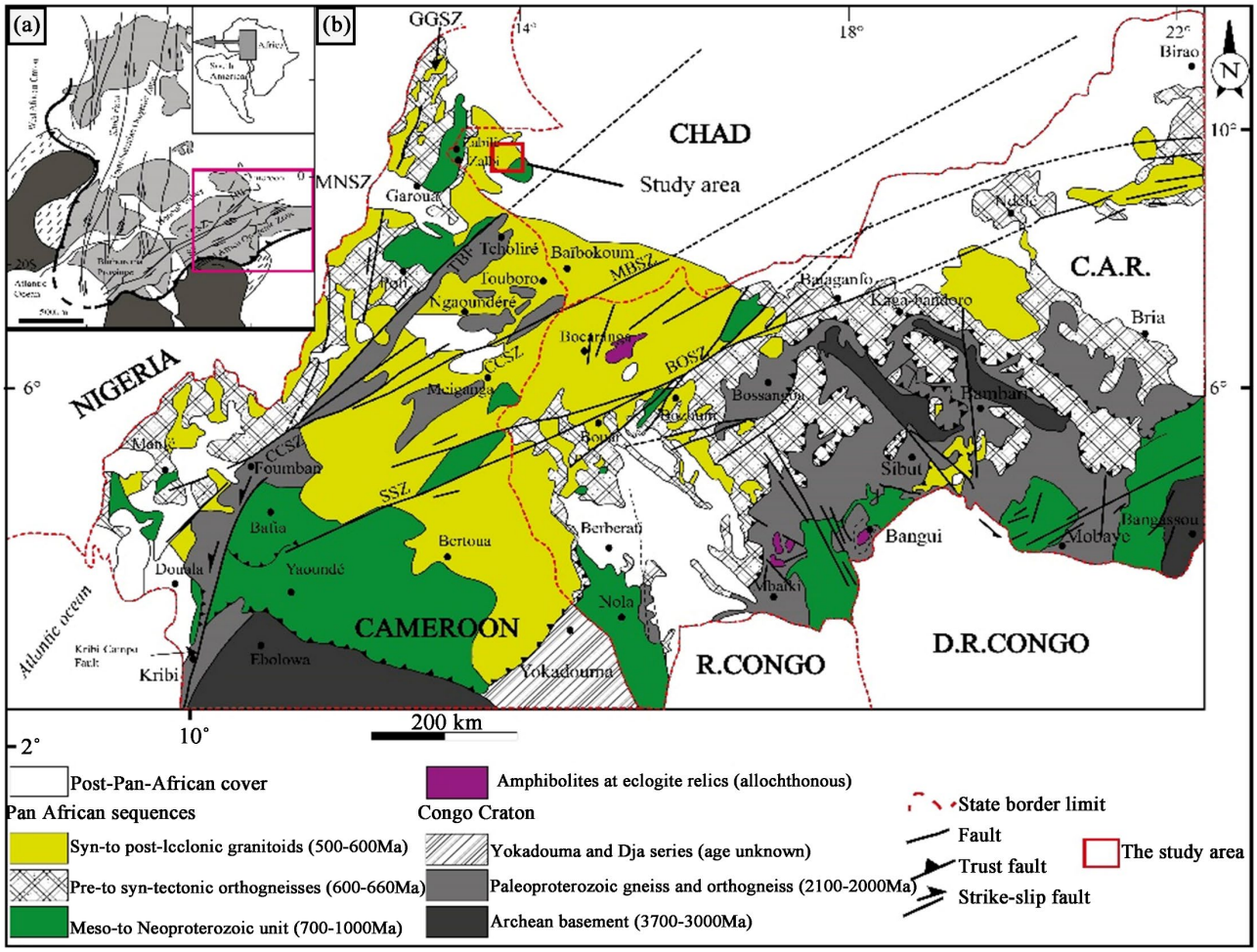

Figure 1. (a) Map of Africa showing he different orogens, craton and central African mobile zone (after [9]); (b) Geological map of Central Africa [10]-[15] showing the main litho-tectonic units and domains of the Central African Fold Belt (SZ: Shear Zone; CCSZ: Central Cameroon Shear Zone; MNSZ: Mayo Nolti Shear Zone; SSZ: Sanaga Shear Zone; MBSZ: M'Bere Shear Zone; BOSZ: Bozoum-Ndele Shear,Zone; TBF: Tchollire Banyo Fault; CAR—Central African Republic; R. Congo: Republic of the Congo; D.R. Congo: Democratic Republic of the Congo).

extending across Nigeria, Cameroon, Chad, and the Central African Republic. The Precambrian formations identified in Chad cover between 15% and 20% of the territory's surface. The Mayo-Kebbi domain is an elongated NE-SW area located between the Central Cameroon and North Cameroon domains. To the south-east it is separated from the Central Cameroon domain by the Massenia-Ounianga gravimetric anomaly, an extension of the Tcholliré Banyo fault (**Figure 2**) [21] [22]. To the northwest it is separated from the North Cameroon domain by the Zalbi volcano-sedimentary series, considered as a northeastern extension of the Poli group [22]-[24]. This domain corresponds to a magmatic arc zone which formed between 800 Ma and 550 Ma by successive collision with the Central Cameroon and North Cameroon domains respectively [4] [22] [25]. It includes 1) greenstone belts, 2) the Mayo-Kebbi batholith, and 3) post-tectonic intrusions [3] [4] [18] [22] [25].

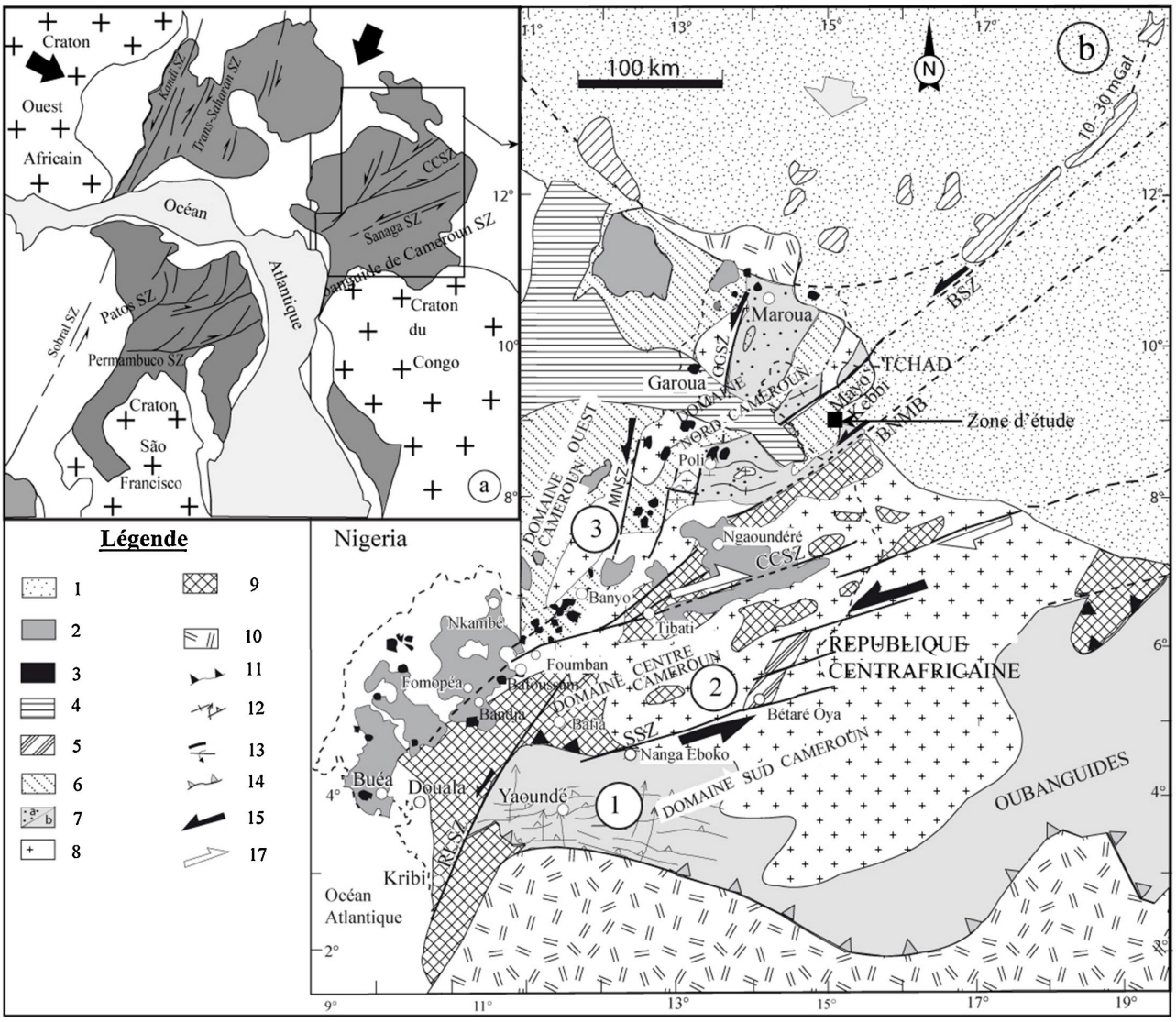

Figure 2. Pan-African structural map of Cameroon [26] and location of the study area. 1: Quaternary sediments; 2: Cameroon Volcanic Line; 3: Cameroon Plutonic Line; 4: Mesozoic sediments (Benue Basin); 5: Lom syntectonic Basin (metasediments, conglomerates, volcanic ash and lavas); 6: West Cameroon Domain (WCD; pre-syntectonic basic to intermediate calc-alkaline intrusions, 660 - 600 Ma); 7a: Poli Group (active Neoproterozoic supracrustal margin and juvenile intrusions); 7b: Yaoundé Group (intracratonic deposits); 8: Late syntectonic subalkaline granitoids; 9: Paleoproterozoic remains of Adamaoua-Yadé and Nyong; 10: Craton (Archean Ntem Complex); 11: Trajectories of S2 foliation and L2 lineation; 12: F2 normal faults and overturned antiforms; 13: Main syn-D2 frontal thrust zone; 14: Syn-D1 thrust zone (separating the low pressure and medium pressure zones in the North from the high pressure zones in the South); 15: Syn-D3 shear direction; 17: Large gray arrows represent the direction of the regional principal stress syn-D1-3. Thick lines: shear zones: BSZ: Balché shear zone; BNMB: Buffle Noir-Mayo Baléo shear zone; CCSZ: Central Cameroon shear zone; GGSZ: Godé-Gormaya shear zone; MNSZ: Mayo Nolti shear zone; RLSZ: Rocher du Loup shear zone; SSZ: Sanaga shear zone.

Covering an area of approximately 10,000 km^2, the Mayo-Kebbi region is located in the southwest of Chad, near the Cameroonian border. It is made up of a crystalline basement. The Mayo-Kebbi domain is an elongated NE-SW complex located between the Central Cameroon and North Cameroon domains. It differs from these two domains by its juvenile Neoproterozoic crust [4] [22] [25]. To the

southeast, it is cut off from the Central Cameroon domain by the Massenia-Ounianga gravity anomaly, an extension of the Tcholliré Banyo fault [22]. To the northwest it is separated from the North Cameroon domain by the Zalbi volcano-sedimentary series, considered as a northeast extension of the Poli group [22] [24] (**Figure 2**). This domain is a magmatic arc zone that formed between 800 Ma and 550 Ma by successive collision with the Central Cameroon and North Cameroon domains respectively [4] [22] [25]. It is composed of 1) greenstone belts, 2) Mayo-Kebbi batholith, and (3) post-tectonic intrusions [3] [4] [18] [22] [25].

- The greenstone belts contain the volcano-sedimentary series (Goueïgoudoum in the East and Zalbi in the West) and the mafic to intermediate complex (metadiorite, metagabbro-diorite and metagabbro) dated around 748 Ma and 700 Ma respectively.

- The Mayo-Kebbi batholith is made up of three generations of granitoids: (i) the syn-tectonic quartzitic metadiorite of the Gauchiot Falls magmatic complex dated at 665 ± 1 Ma, (ii) the hornblende and biotite tonalites dated at 647 ± 5 Ma, and formed by partial fusion of syn-tectonic greenstones and quartz metadiorites; and (iii) the syn-tectonic tonalites dated at 618 Ma. Post-tectonic intrusions are divided into two groups: post-tectonic calc-alkaline potassic granites and alkaline granites. The former are derived from the partial melting of the lower crust (Pouclet et al., 2006). As for the alkaline granites, they are derived from an extreme fractional crystallization of a mantle magma contaminated by an Archean to Paleoproterozoic crust during its ascent [27].

3. Materials and Methods

Data acquisition in the study area focused primarily on a petrographic study. The fieldwork phase allowed for the macroscopic identification of four (4) rock facies (pink granites, pink microgranites, syenites, and granodiorites) and the collection of key lithological parameters, namely color, texture, mineralogical composition, degree of alteration, and deformation. Samples were selected based on their location and lithological relevance.

Rock samples were sawn into chips to prepare thin sections, then cut into small blocks for geochemical studies. Twenty thin sections were thus produced. The petrographic study of the thin sections was carried out at the Dschang Geology Laboratory. The laboratory phase served to refine the petrography. After grouping the main lithological groups constituting the area, this study focused on the geochemistry of granitoids. Eleven rock samples underwent geochemical analyses (major, trace, rare earth elements). These are four (4) pink granites, three (3) pink microgranites, two (2) syenites and two (2) granodiorites. Approximately 200-500 g of each sample was crushed in a steel jaw crusher and then pulverized in an agate ball mill. The powders were digested by alkaline fusion: the powder was mixed with lithium metaborate and melted to produce a glass pellet. This pellet was digested in dilute nitric acid before analyses. Analyses and digestions were carried out at ALS Geochemistry-Loughrea (Ireland). The prepared samples (0.100 g)

were added to a lithium metaborate/lithium tetraborate flux, mixed well, and melted in a furnace at 1000˚C.

The resulting melt is then cooled and dissolved in 100 ml of 4% nitric acid and 2% hydrochloric acid. This solution is then analyzed by ICP-AES and the results are corrected for inter-element spectral interferences. The oxide concentration is calculated from the determined elemental concentration and the result is presented in this form. Whole rock analysis is performed in conjunction with loss on ignition at 1000˚C. The data resulting from both determinations are combined to produce a "total". For the determination of trace elements, the samples were thoroughly mixed and melted in a furnace at 1025˚C. The resulting melt is then cooled and dissolved in an acid mixture containing nitric, hydrochloric and hydrofluoric acids. This solution is then analyzed by ICP-MS.

The elements SiO_2, Al_2O_3, Fe_2O_3, CaO, MgO, Na_2O, K_2O, Cr_2O_3, TiO_2, MnO, P_2O_5, SrO, and BaO were analyzed by ICP-AES (Inductively Coupled Plasma-Atomic Emission Spectrometry). The results were then corrected for spectral inter-element interferences. This analysis is used for certain transition metals (Sc, V, Cr, Ni) and Ba, Cu, and Sr. In contrast, Inductively Coupled Plasma-Mass Spectrometry (ICP-MS) was used to examine the rare earth elements (La, Ce, Pr, Nd, Sm, Eu, Gd, Tb, Dy, Ho, Er, Tm, Yb, and Lu) and for Zr, Hf, Y, Cs, Rb, Th, U, Nb, and Ta.

4. Petrographic Study

4.1. Host Rock

The metamorphic formations consisting of massive amphibolites and quartz chlorite schists constitute the host rock for the formations in the study area. These rocks are collectively known as greenstones [3]. The massive amphibolites outcrop as beds and blocks in the floodplains and as enclaves within the biotite granites. The lateritic coating obscures their contact with the biotite granites. While the quartz chlorite schists are observed as remnants at the quarry site, the contact with the hornblende and biotite granites of Mont Doré is clear.

4.2. Plutonic Formations

The plutonic formations that constitute the rocks of the study area are granitoids. Pink granites, syenites, and granodiorites outcrop as intrusive plutons in the metamorphic rocks: massive amphibolites and quartz chlorite schists constitute the host rocks of the formations. All of these rocks are referred to as greenstones [3] [28] hile pink microgranites outcrop as veins cutting the granodiorites, pink granites, and syenites. Magmatic foliation is not observed on these magmatic formations. Magmatic fluidity is only revealed by the orientation of the enclaves.

4.2.1. Pink Granites

Pink granites outcrop in the form of balls and slabs (**Figure 3(a)**) on the flanks and summits of Mounts Mouta and Gabra, as well as in the surrounding areas. These massive rocks are crossed by dry fractures and sometimes intersected by

Figure 3. (a) Slab outcrop of pink granites from Mount Mouta; (b) Portion of thin section of pink granites. Note the coexistence of orthoclase and microcline crystals, (c) Slab outcrop of pink microgranites to the SW of Mount Gabra, note the presence of microfractures on the slab of pink microgranites; (d) Portion of thin section of biotite microgranites; (e) Block outcrop of syenite from Mount Doré; (f) Portion of thin section of syenite; (g) Enclave of granodiorites in the syenite from Mount Illi; (h) Portion of thin section of granodiorites.

veins of pink microgranites. The pink granites are grainy (Figure 3(a)), leucocratic, and composed of quartz and feldspar crystals. Under the microscope, the texture of these pink granites is porphyritic grainy with jointed crystals. They contain plagioclase phenocrysts ranging in size from 0.125 × 0.25 mm to 1 × 1.5 mm. These rocks are rich in plagioclase, quartz, and microcline; they contain incidental muscovite, chlorite, sericite, epidote, oxides, and sulfides (Figure 3(b)). The mineralogical composition is mainly composed of quartz, plagioclase, alkali feldspar, biotite and muscovite (Figure 3(b)). Accessory minerals are opaques, sphene and apatite. Alkali feldspars are composed of microcline and orthoclase. Orthoclase is in automorphic to xenomorphic sections ranging in size from 0.5 mm × 0.75 mm to 0.75 mm × 1 mm with Carlsbad twinning. Microcline is recognizable by the polysynthetic twins of albite and pericline. Quartz sometimes occurs in aggregates of contiguous crystals arranged in the interstices left by alkali feldspar and plagioclase. Biotite occurs in subautomorphic flakes. Biotite sections are preferentially oriented in the rock. Biotite is included in large alkali feldspar crystals. Plagioclase presents polysynthetic albite twinning (Figure 4). Some crystals present quartz grains in contact with alkali feldspar. Sphene is in rhombic sections attached to biotite flakes. Apatite appears in the form of small rods about 0.125 mm long disseminated abundantly in the rock. Opaque minerals are disseminated in the framework. The opaque ones are in inclusions in the crystals of alkali feldspars, plagioclases and biotite flakes. Chlorite occurs in the form of flakes linked to those of biotite. Muscovite appears in aggregate or in small colorless and limpid crystals.

4.2.2. Pink Microgranites

Pink microgranites outcrop in the form of spheres, slabs (Figure 3(c)), and blocks in the floodplain SE of Mount Gabra, and in the form of centimeter-thick veins cutting through granodiorites, syenites, and pink granites. The pink microgranite has a microgranular texture. Mineralogically, the rock is composed of quartz, plagioclase, alkali feldspar, biotite, and, to a lesser extent, zircon, sphene, and oxides (Figure 3(d)). It is also composed of chlorite. The alkali feldspars are composed of microcline and orthoclase. Microcline is easily identified by the pericline twinning on its edges and is observed as xenomorphic crystals, while orthoclase occurs as augenous to subaugenous patches. Perthitic orthoclase is generally the most abundant. It contains opaque inclusions. Quartz occurs in the framework as subaugenous to xenomorphic crystals. Some quartz crystals are in interstitial form, while others occur as quartz aggregates. Plagioclase crystals exhibit Carlsbad twinning and contain opaque inclusions. Biotite occurs as flakes and contains opaque minerals, apatite, and zircon as inclusions. Apatite is found as an inclusion in alkali feldspar and biotite. Zircon is an inclusion in biotite. Opaque minerals are found alongside plagioclase crystals, alkali feldspar, and biotite flakes. Damourite occurs in the form of xenomorphic crystals.

4.2.3. Syenites

Syenites outcrop in slabs and blocks (Figure 3(e)) on the slopes and summits of

the Doré-Illi Mountains and in the plains. They are broken into blocks ranging from meters to decimeters thick, forming a chaotic landscape. These are dark gray rocks with an orange patina due to weathering. Quartz and feldspars are observed with dimensions ranging from 0.5 cm to 0.75 cm. On a fresh break, more or less chloritized biotite flakes appear. The syenite has a porphyritic grainy texture with alkali feldspar megacrysts. The constituent minerals are: plagioclase, alkali feldspar, quartz, green hornblende and biotite (**Figure 3(f)**). The alkali feldspars are represented in the rock by orthoclase and microcline. The orthoclase crystals are perthitic and show cracks filled with quartz grains. They exhibit microcline destabilization. In sections, the twins form a very fine, almost rectangular, shimmering grid. Plagioclase occurs as subautomorphic to xenomorphic phenocrysts ranging in size from 0.5 × 0.75 mm to 1 × 1.25 mm. It contains opaque minerals as inclusions. Quartz is arranged between the interstices left by other minerals. Green hornblende occurs in longitudinal sections. Some sections contain apatite and opaque minerals as inclusions. Hornblende destabilizes into chlorite. Biotite occurs as elongated flakes and contains inclusions of apatite, zircon, and opaque minerals. Accessory minerals are zircon, sphene, apatite, and opaque minerals. Opaque minerals are very abundant in the rock. Some sections are found as inclusions in orthoclase, plagioclase, biotite, and hornblende crystals.

4.2.4. Granodiorites

At outcrop, granodiorites occur in the form of balls on the slopes of Mount Illi. It should be noted that these rocks locally contain enclaves of massive amphibolite (**Figure 3(g)**). These enclaves are dark gray in color with a grainy texture. Granodiorites are composed of alkali feldspar, quartz, biotite, and amphibole. Granodiorites are mesocratic, with a grainy texture (**Figure 3(g)**). They generally contain abundant feldspar crystals (plagioclase and/or microcline) (**Figure 3(h)**). In addition, crystals of quartz, green hornblende, biotite, chlorite, sericite, epidote, albite, and sphene are present. They also contain ferrotitanium oxides (magnetite and/or hematite). Plagioclase is of low relief. This mineral shows overall subautomorphic to xenomorphic crystals with a size between 0.2 × 0.5 mm and 0.6 × 1 mm. Plagioclase alters into damourite (**Figure 4(b)**). Quartz occurs in the form of xenomorphic crystals with a size varying from 0.3 × 0.5 mm to 0.65 × 0.8 mm. Orthoclase is in the form of automorphic to subautomorphic crystals with an average size of 0.35 × 0.5 mm. Amphibole occurs in elongated or rhombic sections with a size varying from 0.25 × 0.5 mm to 0.65 × 0.5 mm. Biotite overall occurs as yellowish-brown flakes. Opaque minerals are arranged along the cleavages. Biotite contains zircon as an inclusion. Apatite occurs as inclusions in alkali feldspar, plagioclase, and biotite crystals. Zircon occurs as inclusions in biotite flakes. Opaque minerals occur as inclusions in plagioclase, alkali feldspar, biotite, and amphibole crystals. Chlorite occurs as flakes with a greenish coloration.

The relationships between the different mineral phases (**Table 1**) suggest the following crystallization order:

Table 1. Synoptic table of mineral associations of granitoids of the Fianga massif.

Petrographic Set	Petrographic Types	Streckeisen Diagram	Textures	Primary Paragenesis	Secondary Paragenesis
Granitoids	Syenites	Granodiorites	Grenue	Hbl + Bt + Pl + Kfs + Qtz + Ap ± Zr ± Spn	Op + Chl + Da
	Pink granites	Monzo-granites	Grenue	Hbl + Bt + Pl + Or + Qtz ± Zr ± Ap	Chl + Ep + Op + Mc ± Spn
	Granodiorite	Granites alkaline	Grenue Porphy-roid	Bt + Pl + Kfs + Qtz ± Spn ± Zr ± Ap	Chl + Op + Da + Ms
	Pink Microgranites	Microsyeno-granites	Micro-grainy	Bt + Pl + Kfs + Qtz Myr ± Ap ± Zr	Chl + Op + Da

- in granodiorites: accessory minerals, Hbl, Bt, Pl, Kfs, and Qtz;
- in pink granites: accessory minerals, Hbl, Bt, Pl, Or, and Qtz;
- in pink syenites and microgranites: accessory minerals, Bt, Pl, Kfs, and Qtz.

4.3. Microscopic Deformation

Microstructural studies reveal the presence of several types of deformation structures. This deformation is evidenced by the following minerals: plagioclase, alkali feldspar (orthoclase), quartz, biotite, and amphibole. It is composed of submagmatic and post-magmatic deformation (solid-state deformation).

4.3.1. Submagmatic Deformation

Submagmatic deformation corresponds to the deformations acquired by minerals during magmatic crystallization. This deformation is observed in granodiorites, pink granites, and pink microgranites. In these rocks, biotite and feldspar sections exhibit microfractures filled with fine quartz grains. In granodiorites and pink granites, the generally perthitic orthoclase exhibits a microcline transformation.

4.3.2. Solid-State Deformation

Solid-state deformation is reflected in the behaviors exhibited by quartz, feldspar, and biotite sections. In pink granites, syenites, and granodiorites, plagioclase and alkali feldspar exhibit oriented cracks. Quartz is deformed in the form of polycrystalline bands. This indicates high-temperature deformation. Biotite and hornblende are generally destabilized and pulverized as chlorite (**Figure 4(c)**).

4.3.3. Magmatic Deformation

Magmatic deformation results in flow with a preferential orientation of minerals. This deformation is observed in quartz chlorite schists and massive amphibolites.

5. Classification

5.1. Elemental Distributions

The geochemical analysis of the major elements in the rocks studied presents the following four groups of rocks (**Table 2**):

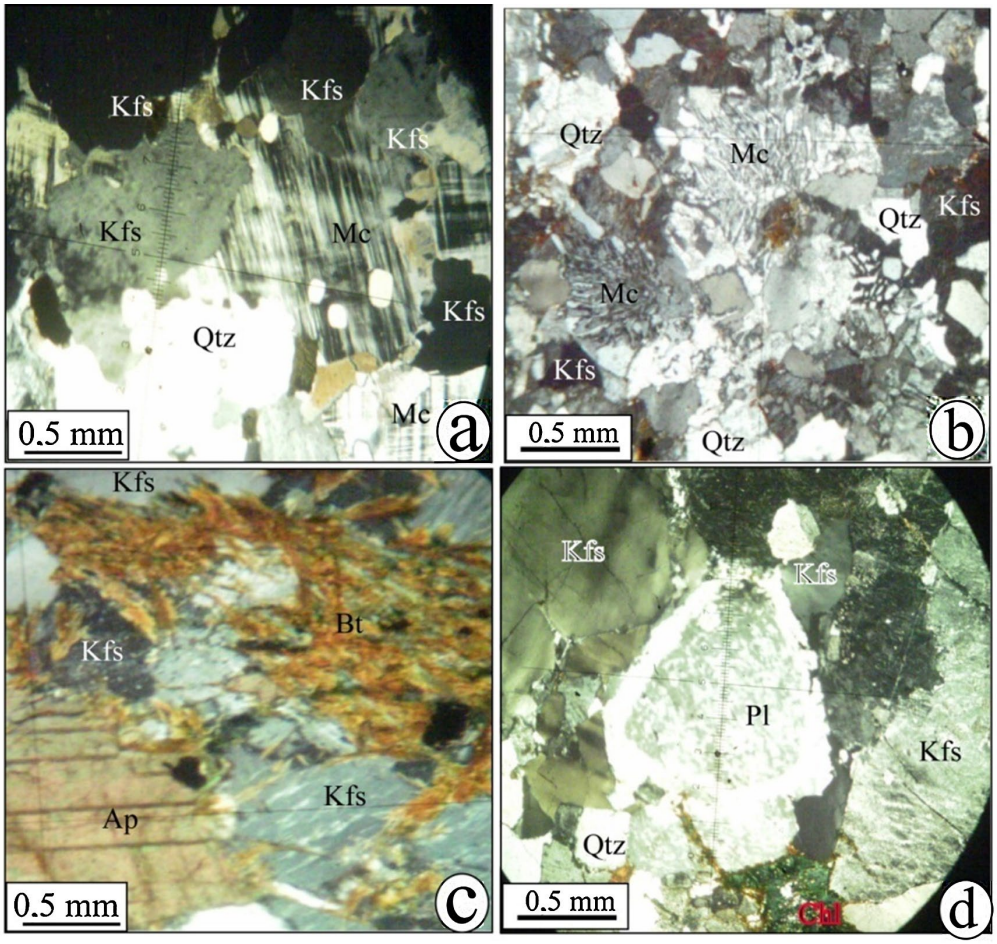

Figure 4. Deformation of minerals under the microscope: (a) coexistence of orthoclase and microcline in syenites, (b) myrmekites bordering alkali feldspars in pink microgranites, (c) biotite destabilized and arranged in orthoclase microfissures in pink granites and (d) plagioclase in the process of destabilization into damourite in granodiorites.

Table 2. Results of geochemical analyses of the Fianga granitoids.

Rock Type	Pink Granites				Pink Microgranite			Syenite		Granodiorite	
Sample	**CE02**	**CE03**	**CE07**	**CE16**	**CE10**	**CE14**	**Fk02**	**R-132**	**R-191**	**CN003**	**MN005**
Latitude (N)	09°93'62"	09°91'63"	09°88'11"	09°85'35"	09°86'13"	09°85'13"	09°90'31"	09°88'34"	09°75'32"	09°79'36"	09°85'53"
Longitude (E)	15°13'33"	15°15'17"	15°11'97"	15°10'73"	15°10'33"	15°99'50"	15°17'44"	15°10'03"	15°10'36"	15°12'39"	15°16'23"
SiO_2	77	77.7	74.9	76.1	78	77.2	75.96	75.644	66.34	75.5	66.2
Al_2O_3	11.9	11.8	11.8	12	12.25	12.4	12.24	0.252	0.395	13.65	15.2
Fe_2O_3	2.31	1.96	2.29	2.13	1.16	1.04	2.07	13.419	17.43	1.3	5.49
FeOt	2.079	1.7636	2.061	1.9166	1.0438	0.936	1.8626	12.074	15.69	1.1697	4.9399
MnO	0.05	0.04	0.05	0.05	0.04	0.02	0.04	1.502	3.288	0.01	0.08
MgO	0.13	0.09	0.27	0.26	0.04	0.04	0	0.008	0.072	0.09	1.26
CaO	0.81	0.63	1.32	1.1	0.29	0.55	0.16	0.193	1.199	0.93	2.92
Na_2O	4.24	4.32	4.17	4.09	4.37	3.95	4.2	<LD	3.678	3.93	4.17

Continued

K_2O	3.57	3.75	3.35	3.48	4.37	4.76	3.89	3.836	5.226	4.85	3.68
TiO_2	0.18	0.15	0.2	0.2	0.05	0.06	0.13	4.812	2.106	0.07	0.83
Cr_2O_3	0.034	0.025	0.025	0.019	0.028	0.025				0.009	0.005
P_2O_5	0.01	0.01	0.03	0.03	0.01	0.01	0.05	0.025	0.137	0.02	0.26
Mg#	10.09	8.3915	19.04	19.582	6.4362	7.126	0	0.1188	0.817	12.135	31.406
LOI	0.62	0.33	1.03	0.58	0.4	0.36	0.6	0.713	0.578	1.09	1
Total	100.9	100.81	99.44	100.04	101.01	100.4	99.79	100.4	100.5	101.47	101.2
Trace elements (ppm)											
Sc		44.8	80.9	68.7	7.1	21	9.3	1.86	0.68	1	7
V	8	<5	14	17	<5	<5	4	5.8	52.4	11	54
Co	1	<1	1	1	1	<1	18	0.94	6.47	2	13
Ni	2	1	2	2	1	<1	18	3.5	6.7	7	13
Ga	25.8	26.6	22.3	23.5	30.9	21.1	24.1	20.1	21.6	18.4	26.6
Rb	70.5	80.8	56.5	81.2	245	116.5	88	117.4	33.2	219	182
Sr	61.1	44.8	80.9	68.7	7.1	21	41	47.2	786.6	53.5	286
Rb/Sr	1.154	1.8036	0.698	1.182	34.507	5.548	2.1463	2.4873	0.042	4.0935	0.6364
Y	97.5	110	84.9	86.4	103	66.6	89.5	264	120.5	9.2	32.1
Zr	286	288	254	257	121	102	256	264	120.5	83	411
Nb	16.55	19.3	16.55	17.35	53.2	13.8	16.9			15.35	32.9
Sn	4.3	5	4.2	4.7	18.8	4.7		4.32	0.69	1	5.3
Cs	1.66	1.62	2.95	2.89	4.85	1.95	9.3	1.86	0.68	10.25	9.83
Ba	988	859	849	797	44.5	213	876	454.6	957.6	91.2	533
La	40.3	40.3	35.5	37.4	16.4	17.8	30.1	28.77	11.58	32.911	285.23
Ce	92.8	95.9	82.4	86.9	44	37.4	74.6	51.59	26.05	23.491	215.33
Pr	12.25	12.6	10.8	11.35	5.95	5.35	10.5	7.595	3.086	18.534	160.02
Nd	53.9	56.1	47.3	48.9	23.9	22.6	48.4	27.45	11.48	13.129	116.63
Sm	13.85	14.3	12.35	12.55	6.64	6.09	13.9	5.917	2.09	11.554	63.176
Eu	2.21	2.14	1.81	1.92	0.13	0.28	2.15	0.714	0.715	3.73	26.465
Gd	15.35	16.3	13.9	13.6	8.23	7.24	13.3	5.541	1.597	6.3317	37.286
Tb	2.64	2.9	2.35	2.38	1.78	1.38	2.34	1.05	0.223	4.9861	30.471
Dy	16.85	18.5	15.4	15.05	12.9	9.38	14.3	7.041	1.228	5.1626	24.309
Ho	3.45	3.85	2.99	3.08	2.94	2.05	3.07	1.449	0.228	4.7619	19.78
Er	10.4	11.85	9.49	9.62	10.95	6.73	8.91	4.423	0.638	5.625	19.688
Tm	1.59	1.79	1.45	1.46	2.1	1.14	1.44	0.736	0.103	0.001	17.004
Yb	9.71	11.4	9.09	9.34	16.1	7.69	9.56	5.256	0.787	8.3851	18.82

Continued

Lu	1.52	1.78	1.44	1.52	2.76	1.3	1.45	0.81	0.133	54.878	123.17
Hf	9.83	10.4	9.16	9.41	10.9	5.35	8.95	8.124	3.177	3.94	11.1
Ta	1.1	1.2	1.2	1.2	5.2	1.5	1.36	2.17	0.374	2.1	2.7
W	1.2	1	0.8	1.5	1.6	3	1.88	<LD	<LD	19.2	21.6
Th	5.94	6.84	6.19	7.45	22.2	11.55	9.598	1.016		25.8	37.6
U	1.71	2.02	2.26	2.49	9.27	3.79	3.845	0.447		13.45	7.77
Ti	0.11	0.09	0.12	0.13	0.03	0.04	1512	2370			0
Cr	233	166	171	125	194	172	4.7	7		68	35
Ag	<0.5	<0.5	<0.5	<0.5	<0.5	<0.5				<0.5	<0.5
As	<5	<5	<5	<5	<5	<5				<5	7
Cd	<0.5	<0.5	<0.5	<0.5	<0.5	<0.5					
Cu	3	6	12	3	2	8				9	20
Li	<10	10	10	10	<10	<10				<10	40
Ni	2	1	2	2	1	<1		3.5	6.7	7	13
Pb	11	10	13	12	23	13	9.48	16.9	8.89	32	19
Zn	118	123	105	108	76	32		40.1	79.7	11	75
Ti	1079	899.25	1199	1199	299.75	359.7	779.35	28848	12625	419.65	4975.9
K	29636	31130	27809	28889	36277	39514	32292	31844	43383	40261	30549
(Dy/Yb)N	1.136	1.0621	1.109	1.0546	0.5244	0.798	0.979	0.8767	0.403	0.8454	1.0212
(La/Sm)N	1.817	1.7599	1.795	1.861	1.5424	1.825	1.3523	3.0363	1.779	2.8194	3.46
(Ce/Yb)N	2.51	2.2094	2.381	2.4436	0.7178	1.277	2.0495	2.578	0.736	3.0051	8.6936
(La/Ce)N	1.123	1.0869	1.114	1.1132	0.9641	1.231	1.0436	1.4424	3.624	3.4261	1.1498
(La/Yb)N	2.819	2.4015	2.653	2.7202	0.692	1.572	2.1389	3.7185	2.666	10.296	9.9957
(Gd/Yb)N	1.279	1.1568	1.237	1.1781	0.4136	0.762	1.1256	0.8529	0.611	1.6029	1.6417
Eu/Eu*	0.462	0.4273	0.421	0.448	0.0536	0.129	0.482	0.3801	1.329	1.6622	1.193
Ce/Ce*	1.01	1.0296	1.018	1.0204	1.0776	0.927	1.0152	0.8443	0.23	0.2438	1.0542

- In the pink granites of Fianga, SiO_2 contents range from 74.29% to 77.7%; Na_2O from 4.09% to 4.32%; K_2O from 3.35% to 3.75%. The high Al_2O_3 contents (11.8 to 12%) reflect the high plagioclase content in this facies. The Na_2O/K_2O ratio of 1.15 to 1.24 is characteristic of rocks that are more sodic than potassic. Their variable contents of CaO (0.63% to 1.32%), Rb (56.5% to 81.5%), and Sr (44.8% to 80.9%) are related to the degree of plagioclase alteration. This high degree of alteration is also expressed by the high loss on ignition content (0.33% to 1.03%). Iron, with contents varying from 1.96% and 5% to 2.31%, comes from biotite, the only ferromagnesian mineral of this facies, and from chlorite.

- Compared to the previous pink granites, the pink microgranites show higher

contents of silica SiO_2 (77.2% to 78%), Al_2O_3 (12.25% to 12.4%) and K_2O (4.37% to 4.76%) and lower contents of Fe_2O_3 t (1.04% to 1.16%), MgO (0.04%), CaO (0.26% to 0.55%) and TiO_2 (0.05% to 0.06%). The Na_2O/K_2O ratio is between 0.82% and 1.07%. These ratios characterize the more sodic than potassic rocks. These pink microgranites are richer in Rb (88 to 245 ppm), Zr (102 to 256 ppm), Ba (44.5 to 876 ppm), U (3.28 to 9.27 ppm) and Th (9.59 to 22.2 ppm), and poorer in Zn (0 to 76 ppm) and Ta (1.36 to 5.2 ppm).

- Syenites are more differentiated than other facies. They are distinguished by higher SiO_2 contents (75.5% to 75.64%) and lower Al_2O_3 contents (0.25% to 13%), CaO (0.19% to 0.93%), MgO (0.008% to 0.09%), Fe_2O_3t (1.3% to 13.41%) and TiO_2 (0.04% to 4.8%). The Na_2O/K_2O ratio is 0.703% to 1.133% and characterizes potassic rocks rather than sodic ones. It also shows higher Nb (15.33 ppm), Zr (83 to 264 ppm) and Ta (2.1 to 2.17 ppm) contents. Higher Rb contents (117.4 to 219 ppm), and low Ba (91.2 to 454.6 ppm), and Sr (47.2 to 53.5 ppm) contents are related to lower plagioclase and alkali feldspar rates compared to these facies. Their more differentiated character is also marked by lower transition element V contents (5.8 to 11 ppm).

- Granodiorites are distinguished from other facies by higher SiO_2 (66.2% to 66.34%), K_2O (3.68% to 5.22%); Na_2O (3.67% to 4.17%) and lower Al_2O_3 (0.39% to 15.2%) contents. These low CaO contents (1.19% to 2.92%) are accompanied by high Sr contents in other samples reaching 786.6 ppm. TiO_2 and P_2O_5 contents vary from 0.83% to 2.10% and 0.13% to 0.26%, respectively. These contents reflect the low levels of ferromagnesian minerals and plagioclase in this facies. The ratio (Na_2O/K_2O) is equal to 0.810% and is characteristic of rocks more potassic than sodic. These rocks have lower contents than pink granites in Nb, Zr, Zn and higher in Ba (533 to 957.6 ppm).

In the classification diagram of the studied rocks $K_2O + Na_2O$ vs SiO_2 [29]; (**Figure 5(a)**), all pink granites, microgranites and a sample of syenites are plotted in the field of granites with the exception of granodiorite samples which are placed respectively in the quartz monzonite domain and a sample of syenite which is in the granodiortes domain. In the diagram (A/NK vs A/CNK) of Maniar and Piccoli [30], all the studied rocks are found in the domain of peraluminous granitoids and S-type granites (**Figure 5(b)**). This character is confirmed by the diagram of Maniar and Piccoli [30] (**Figure 5(d)**). This diagram also clearly separates metaluminous granitoids, whose A/NK ratio is defined as an $Al_2O_3/(Na_2O + K_2O)$ molar ratio greater than 1, and peralkaline granitoids (A/NK < 1). All the studied rocks are located in the peraluminous domain except for one syenite sample and one pink microgranite sample which are found in the metaluminous domain. The position of these samples could be explained by their mineralogy; they are rich in alkaline minerals (e.g., potassium feldspar) which lower the $Al_2O_3/(Na_2O + K_2O)$ ratio.

5.2. Variation of Major Elements

In the various oxide diagrams as a function of SiO_2 (**Figure 6**), the different

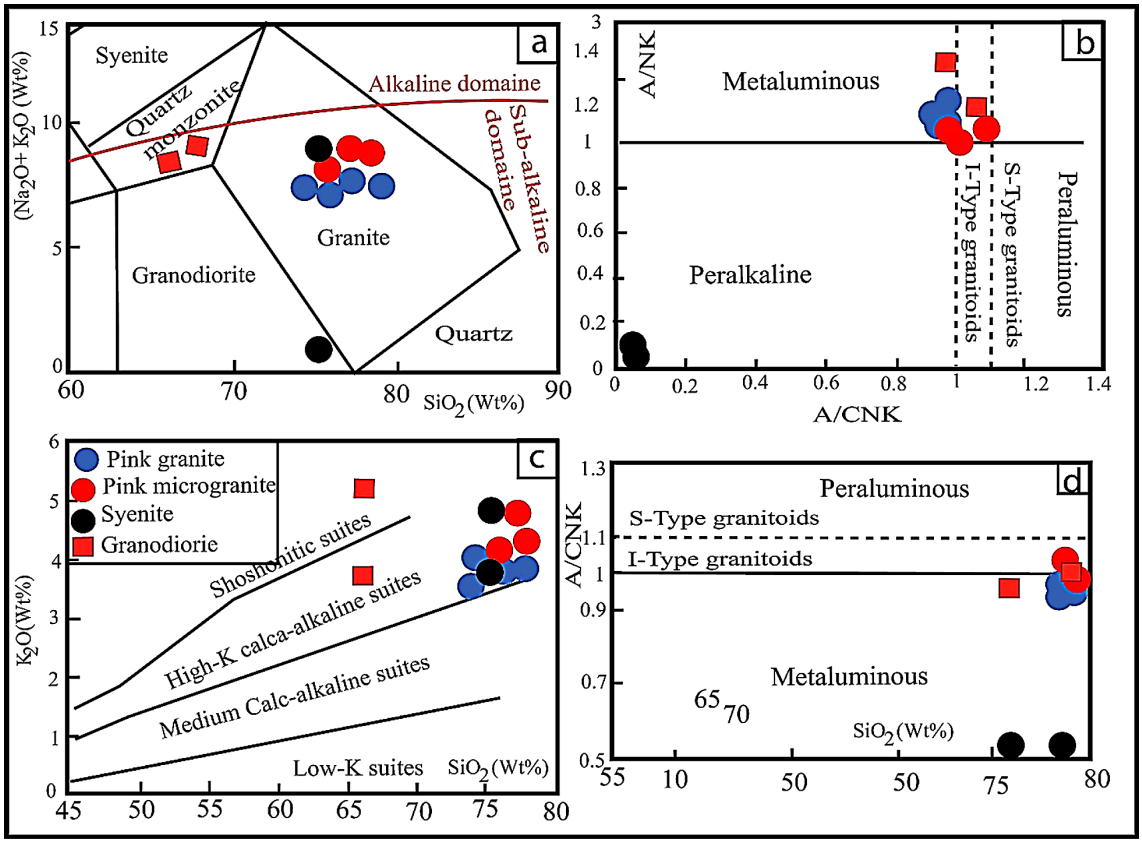

Figure 5. (a) Classification of the rocks studied in the diagram of $Na_2O + K_2O$ vs SiO_2 [29], (b) Fianga granitoids in the diagram (A/NK vs A/CNK) of Maniar and Piccoli [30]; A/NK: $Al_2O_3/(Na_2O + K_2O)$, A/CNK: $Al_2O_3/(CaO + Na_2O + K_2O)$, (c) Classification of Fianga rocks in the K_2O vs. SiO_2 diagram with compositional domains of the different calc-alkaline series [31]; (d) (Peraluminous characteristics of the Fianga rocks. (a) Aluminum saturation index, A/CNK = $Al_2O_3/(CaO + Na_2O + K_2O)$ molar as a function of SiO_2 (mass %). The boundary separating the metaluminous and peraluminous domains (solid line) is that of Chappell and White [32], while the dotted line dividing the peraluminous domains into weak and strong is that summarized by Zen [33]. In this K_2O vs SiO_2 diagram of Pecerillo and Taylor [31], all the granitoids studied occupy the strongly elevated potassic domain (**Figure 5(c)**). The generally potassium-rich character of the studied rocks is consistent with their Al_2O_3 content greater than 9%) [34] [35] and with their notable abundance of potassium feldspar (and therefore K_2O).

compatible elements generally define a trend of decreasing evolution with increasing SiO_2. These rocks appear to evolve following the same process. However, a peculiarity is noted in certain diagrams. MgO, CaO, P_2O_5, TiO_2, and Fe_2O_3 show a decrease in content from granodiorites to pink granites. Na_2O, K_2O, and Al_2O_3 show an increasing trend from granodiorites to pink granites. In the various diagrams, pink granites, pink microgranites, and syenites are intercalated. The behavior of the alkali elements Na_2O and K_2O confirms these trends. However, some elements have a high oxide content. The large variation in Al_2O_3 (0.252% - 15.2%) suggests a correlation with silica (**Figure 6**).

5.3. Trace and Rare Earth Elements

Pink granites have lower values of Ba (797 - 988 ppm), low Sr (44.8 - 80.9 ppm), and low Rb (56.5 - 81.2 ppm). Pink microgranites have relatively lower values of

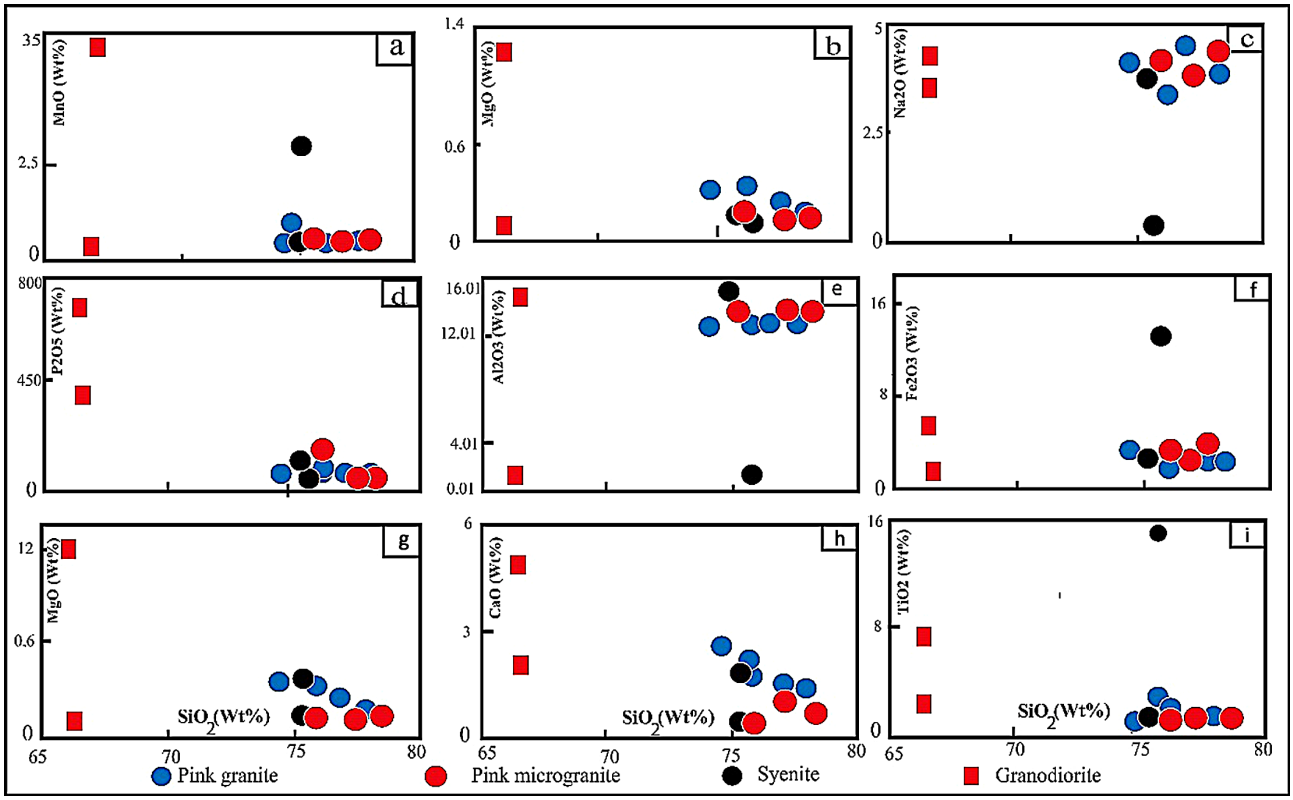

Figure 6. Harker diagram of major element concentrations versus SiO_2 in granitoids.

Ba (44.5 - 876 ppm) and very low Sr (7.1 - 41 ppm) and Rb (88 - 245 ppm). Syenites have low values of Ba (91.2 - 454.6 ppm), Sr (47.2 - 57.3 ppm), and Rb (117.1 - 219 ppm). Granodiorites have slightly elevated values of Ba (553 - 957.6 ppm), high Sr (286 - 786.6 ppm), and low Rb (33.2 - 182 ppm). In the different diagrams of oxides as a function of SiO_2 (Figure 6), the different incompatible elements generally define a trend of decreasing to increasing SiO_2 evolution. These rocks appear to evolve following the same process. However, a particularity is noted in certain diagrams. Zr, Sr, Ta, and Nb show a decrease in content from granodiorites to pink granites. Zn, Ba, Y and Rb show an increasing appearance going from granodiorites to pink granites. In the different diagrams, pink granites, pink microgranites, syenites and granodiorites are intercalated. The Rb/Sr ratios are low in pink granites (0.69 - 1.80), high in pink microgranites (2.14 - 34.50), moderately high in syenites (2.48 - 4.50) and very low in granodiorites (0.04 - 0.63).

6. Discussion

6.1. Petrogenetic Process

The enrichment in Rb, Ba, and K, and the high K/Nb and La/Nb ratios are consistent with crustal-derived enrichment fluids. Compared to mid-ocean ridge basalts, the subducted sediments are highly enriched in several interesting elements, including moderately enriched K, Rb, Sc, Ba, Sr, U, Th, Pb, Sm, Nd, Lu, and Hf. During differentiation, the LREE content increases (the latter are incompatible in

some minerals), while the HREE contents stagnate during differentiation (amphibole effect, clinopyroxene). The negative Europium anomaly is characteristic of granitoids, which confirms that plagioclase crystallizes late in the differentiation series of tholeiitic magmas in general (Figure 7).

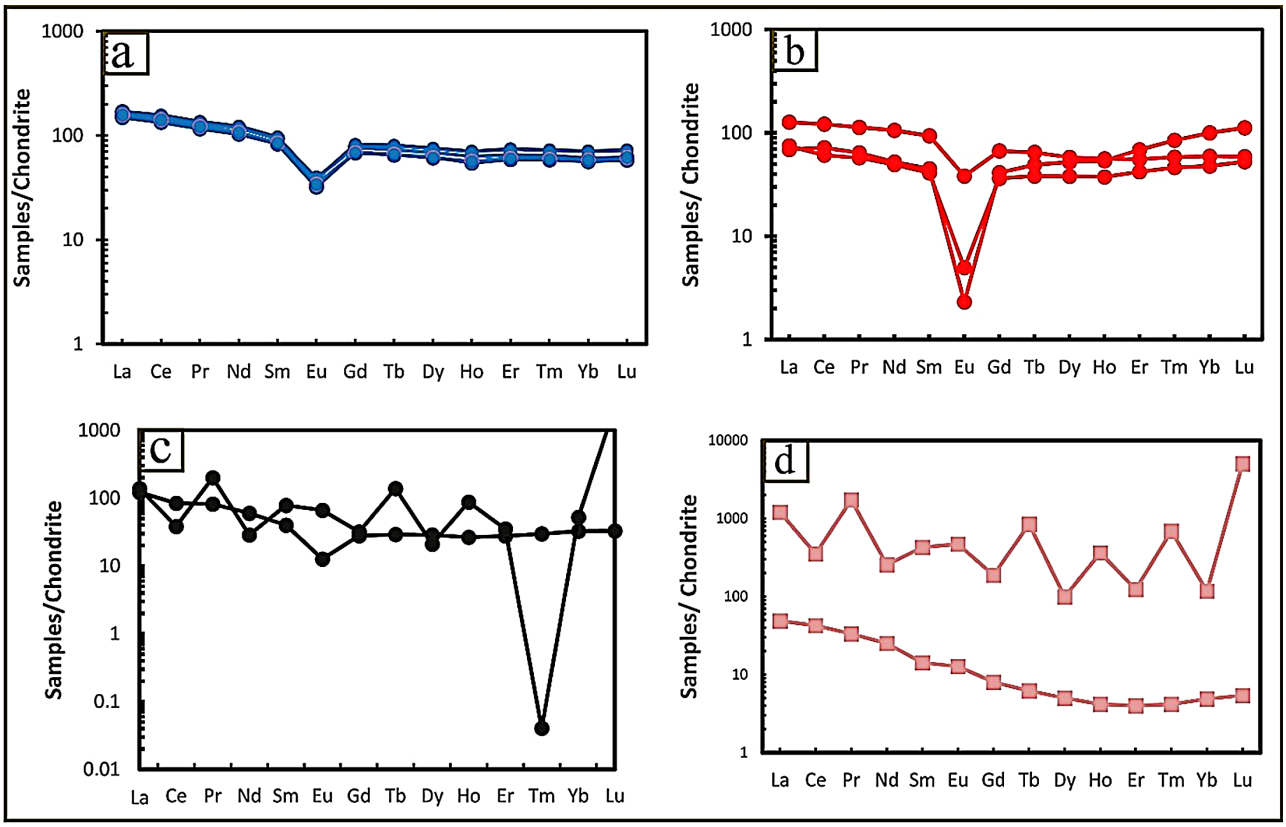

Figure 7. Rare earth spectra of Fianga granitoids normalized to chondrites [36]: (a) Pink granites, (b) Pink microgranites, (c) Syenites and (d) Granodiorites.

Large ion lithophile elements (LILE) and high field strenght elements (LREE) enrichment in the Fianga granitoids has been shown to result from enrichment from an ancient lithospheric source and not from crustal contamination during ascent. Rare earth elements have generally played an important role in the characterization and identification of the processes responsible for incompatible element enrichment in mantle rocks. The high Ba/Nb ratios (5.94 - 53.83) suggest a subduction or shear environment for the source enrichment of the Fianga rocks. Indeed, in the Nb/Yb vs. Th/Yb diagram (Figure 8(a)) the Fianga rocks are predominantly from the mantle system. Dans le diagramme Ba/La vs. Th/Yb (Figure 8(b)), les granitoïdes sont issus de la fusion partielle de MORB. Furthermore, the Fianga rocks exhibit relatively high Nb/Zr ratios and low Rb/Y ratios (Figure 8(c) and Figure 8(d)), characteristics similar to magmas produced by the interaction between planar-derived fluids and subarctic mantle peridotites [37]. The Fianga rocks have a medium Nb/Zr ratio, indicating that they were enriched during melting. This suggests that Th enrichment may be fluid-mediated.

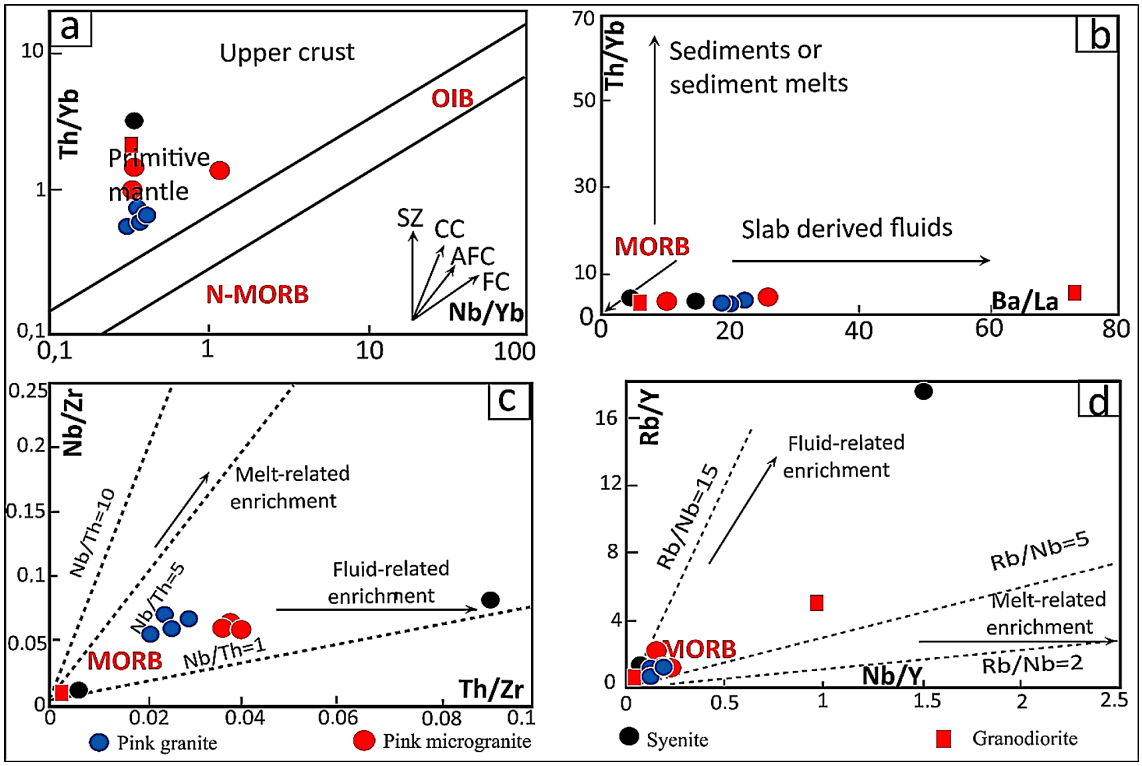

Figure 8. (a) Nb/Yb vs. Th/Yb diagram shows the importance of subduction environment in the generation of syenitic pluton magma (SZ: subduction zone, CC: continental crust, AFC: assimilation fractional crystallization, FC: fractional crystallization); (b) Ba/La vs. Th/Yb; (c) Nb vs. Th/Zr and (d) Rb/Y vs Nb/Y diagrams after [37] show the influence of slab derived fluids during the generation of the syenitic pluton magma.

The rocks in the study area are derived: (i) either from a mixture of acidic and basic magmas with the intervention of crustal assimilation and fractional crystallization processes [38] [39], (ii) or by the process of assimilation coupled with fractional crystallization (AFC) (**Figure 9(d)**). This process has been widely accepted to explain the genesis of several plutons worldwide [40]-[43]. The source of alkaline-potassium magmatism is linked either to the melting of a crust or to the partial melting of the enriched subcontinental lithospheric mantle [41] [44]. These geochemical features indicate that the granitoids may have formed by partial melting of metasomatized mantle in a post-collisional subduction setting [45] [46]. The high La/Nb (0.30 - 8.66) and low La/Ba (0.012 - 0.36) ratios of these granitoids are consistent with their origin by partial melting of subduction-modified subcontinental lithospheric mantle [47] [48].

6.2. Crystallization

Harker diagrams and rare earth element distribution patterns suggest that fractional crystallization played an important role in the differentiation of the pluton rocks. Furthermore, the distribution of MgO, Fe_2O_3, and MnO with SiO_2 indicates the fractional crystallization of clinopyroxene and hornblende. The moderate Ba content and the weak negative Eu anomaly are consistent with K-feldspar fractionation. Compared to primitive mantle magmas, the highly variable MgO, mag-

nesium number (Mg #: 32.8 - 62.6), and transition element (Sc, Cr, Co, Ni) contents of the studied granitic rocks suggest that some degree of fractional crystallization occurred during granitoid emplacement [19] [49] [50]. These sufficiently high contents in these rocks demonstrate that the primary magmas underwent fractional crystallization [19] [49]-[51]. The behavior of trace and major elements is consistent with the crystallization of amphiboles and plagioclases, which are the most important mineral phase. In detail, the progressive decrease in TiO_2 and Fe_2O_3 contents is related to the continuous fractionation of ferro-titanium oxides. The decrease in Al_2O_3 and Sr contents is the result of the significant fractionation of plagioclase feldspars. It is important to note that the increase in Al_2O_3 contents and the negative Eu anomaly in the rare earth spectra of granitoids is consistent with the presence of plagioclases in thin sections (5% - 10%) and consequently the crystallization of mafic minerals. The high Ba and Rb contents indicate the significant crystallization of alkali feldspars in granitoids as well as suggest metasomatism or crustal contamination. The magmas, rising towards the surface, would have evolved by fractional crystallization while assimilating part of the continental crust, i.e. by the process known as AFC (assimilation coupled with fractional crystallization) [19] [50]-[52]; **Figure 9(d)**). The AFC phenomenon

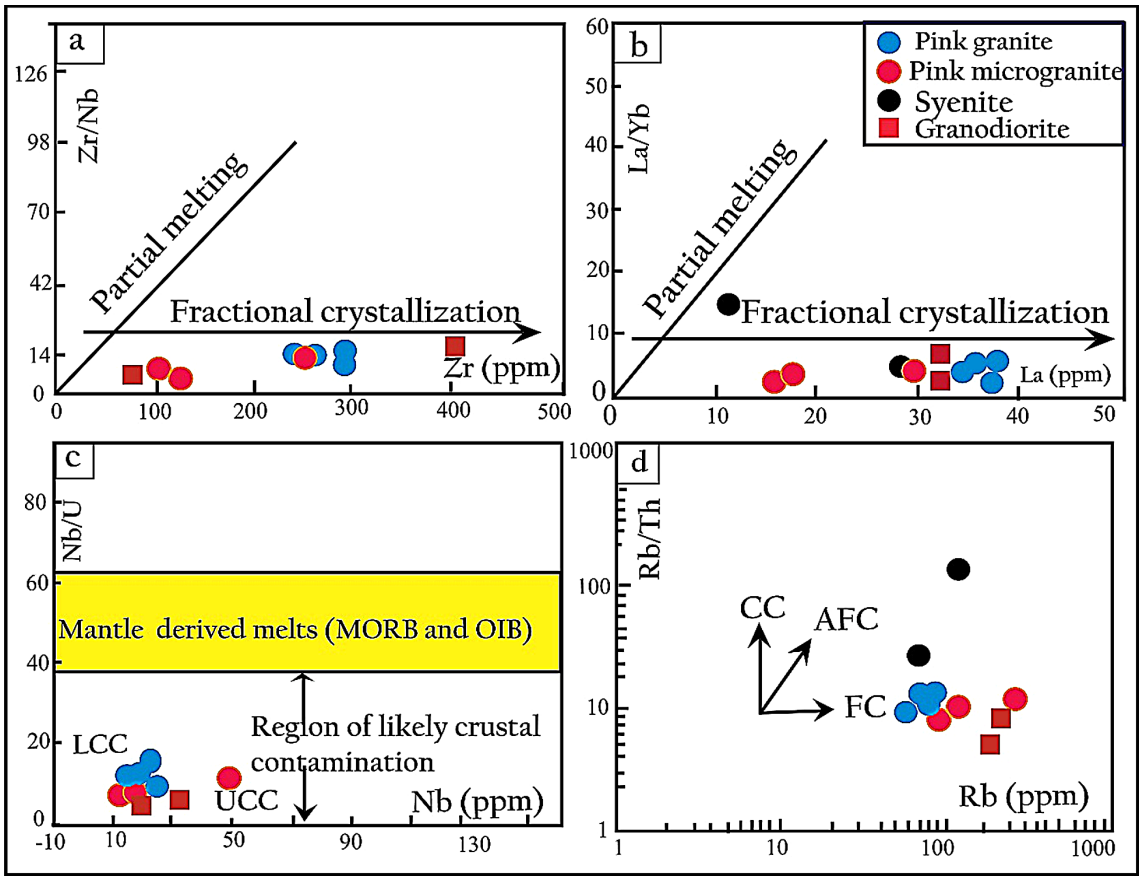

Figure 9. Discrimination of magmatic differentiation process: (a) Zr vs. Zr/Nb, (b) La vs. La/Yb [53]; (c) Nb vs. Nb/U [54]; (d) Rb vs. Rb/Th [55]. AFC; assimilation-fractional-crystallization; CC: crustal contamination; FC: fractional crystallization.

helps explain the presence of syenites between pink granites and granodiorites.

In the trace element diagrams as a function of Zr, Rb and La highlighting fractional crystallization (**Figure 9(a)**, **Figure 9(b)** and **Figure 9(d)**). This behavior of the rocks suggests the presence of a single alkaline magma from a deep source (mantle) that would be at their origin. These correlations indicate that the magmas at the origin of the granitoids probably came from the same source. Collinearities of trace element variations shown by the different diagrams (**Figure 9(a)**, **Figure 9(b)** and **Figure 9(d)**) also indicate the development of fractional crystallization processes operating in more or less enriched and/or contaminated mantello-derived magmas. In the Nb vs. Nb/U diagram (**Figure 9(c)**), we note that the granitoids originate from the partial melting of the lower continental crust.

6.3. Geochemical Affinity

The Fianga pink granitoids are predominantly alkaline, sodic rocks with a K_2O/Na_2O ratio ≤ 1. Pink granites (A/CNK = 0.91 - 0.96), pink microgranites (A/CNK = 0.98 - 1.07), syenites (A/CNK = 0.02), and granodiorites (A/CNK =0.94 - 1.40) are metaluminous to peraluminous. This process has been widely accepted to explain the genesis of several alkaline plutons worldwide [41]-[43] [46] [56]. The source of high-potassic alkaline magmatism is related either to crustal melting or to partial melting of the enriched subcontinental lithospheric mantle [43] [44]. However, these rocks generally contain magnesium number (Mg#) rich mafic minerals (0.11 - 31.40) such as diopside, magnesiohornblende, and magnesian biotite. These characteristics could exclude their grouping as alkaline rocks. On the other hand, K_2O is more or less high than Na_2O (K_2O/Na_2O = 0.84 - 1.42, mean = 0.922) in the study rocks and the fact that they are found in the high K field on a K_2O vs SiO_2 diagram (**Figure 5(c)**) suggests that these rocks have a rather high potassium affinity, i.e., for their SiO_2 values, they are higher than usual in K_2O [57]. Geochemical analysis shows that the granitoids are Type-I, metaluminous to peraluminous. The enrichment of LREEs relative to HREEs (LaN/YbN = 0.69 - 10.29) and the flat profile of HREEs lead us to propose a spinel-lherzolite peridotite as a mantle source [58]. The balance of moderately incompatible elements (HREE, HFSE, and Ti) is largely controlled by partial melting processes [59]. In particular, HFSE are used to constrain the nature of mantle sources that may have been depleted by previous melt extraction in back-arc basins or in the arc environment [60]. However, Nb/Ta and Zr/Hf ratios can be significantly fractionated and positively correlated during partial melting of the lower mantle. This process should also lead to positive correlations between subchondritic Nb/Ta ratios and La/Yb, Th/Yb, and Y/Sc ratios, which would decrease with increasing mantle wedge depletion [59]. However, the Fianga granitoids do not show such correlations (**Figure 10**), suggesting that their region of source was a rather primitive lithospheric mantle, which had not been depleted by previous extraction of molten material [59].

The Nb/U (<30) and Nb/Th (<8) ratios of the Fianga pluton rocks are close to

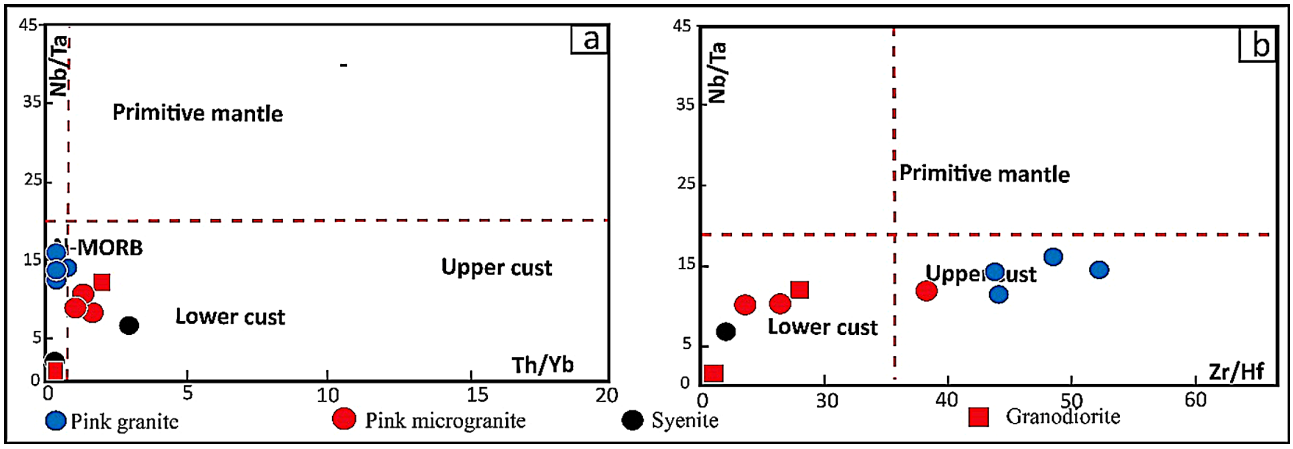

Figure 10. Plots of Nb/Ta vs. Th/Yb (a) and Nb/Ta vs. Zr/Hf, (b) for the Fianga granitoids. N-MORB, OIB, and primitive mantle values are from Sun and McDonough [61]. Nb/Ta ratios are constant around 31, the primitive mantle value.

the values of the primitive mantle. Therefore, the LREE enrichment suggests an enriched source in the mantle rather than an evolved magmatic process. The granitoids have Sm/Yb ratios above the spinel-lherzolite melting curve, but below the garnet-lherzolite melting trend, so that all analyzed samples lie between the two trajectories on the E-MORB side (**Figure 11(b)**) except for one granodiorite sample. In the La/Sm vs. La diagram (**Figure 11(a)**), most samples lie between the garnet-lherzolite and spinel-lherzolite curves, suggesting that they originate from a mantle reservoir, slightly deeper than the garnet-spinel lherzolite level. This source region is expected to be located in the spinel lherzolite and garnet lherzolite transition zone corresponding to depths of about 70 - 80 km [59]. This postulate can be confirmed by the $(La/Yb)_N$ ratio. A $(La/Yb)_N$ ratio < 5 identifies a mantle composed of spinel lherzolite, while a $(La/Yb)_N$ ratio > 5 is characteristic of a mantle composed of garnet lherzolite [61]. This ratio is high in granodiorites ($9.99 < (La/Yb)_N < 10.25$), therefore the source is a mantle composed of garnet lherzolite. Conversely, this ratio is low in roceogranites, pink microgranites, and syenites ($0.69 < (La/Yb)_N < 3.71$). This ratio demonstrates that a mantle composed of spinel lherzolite would be the source of these rocks. This study reveals a mantle source composed of spinel-garnet lherzolite that could be the origin of the rocks studied.

The rocks of the Fianga pluton crystallized from weak partial melting (**Figure 11(c)**). This low degree of partial melting is consistent with their high HFSE contents and high $(La/Yb)_N$ ratios. The relatively high K_2O/La ratios (0.012-0.451) but low U/La ratios (0.015 - 0.565) in the rocks of the study area may also be consistent with a lithospheric mantle of similar composition to garnet lherzolite followed probably by modification by lower crustal contamination or subduction zone enrichment.

6.4. Crustal Contamination

Crustal contamination may play a role in the petrogenesis of magmas as they breach the continental crust in the case of plutons. Fractional crystallization

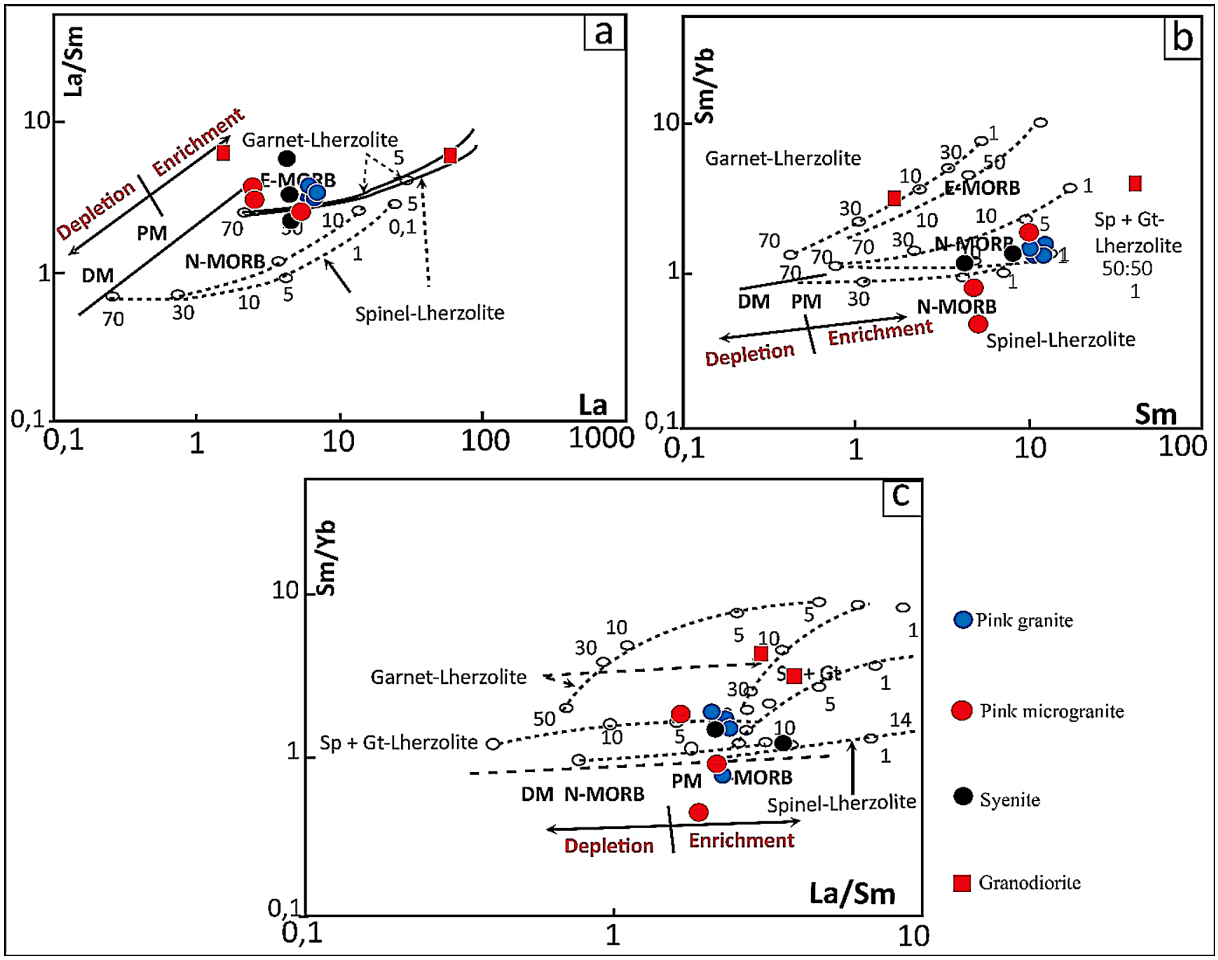

Figure 11. Rare earth element variations in the Fianga granitoids (a) La/Sm vs La, (b) Sm/Yb vs Sm and (c) Sm/Yb vs La/Sm. Mantle lattice defined by the compositions of the MORB-depleted mantle [58] and the primitive mantle [61]. Melting curves for spinel-lherzolite and garnet-lherzolite sources of DM and PM compositions from [62]; circled points on each melting curve correspond to the degrees of partial melting for a given mantle source. The N-MORB and E-MORB compositions of Sun and McDonough [61] are also shown.

associated with crustal contamination (FCC) is an important process during magma evolution [52]. It can modify the elemental compositions of magmas. Crustal materials are rich in LILE, K2O, and Na_2O and depleted in P_2O_5 and TiO_2. Therefore, crustal contamination will increase significantly with K_2O, Na_2O, and LILE. The lower K_2O concentrations and variable Na_2O concentrations in rocks suggest low crustal contamination with a K_2O/Na_2O ratio ≤ 1. The cause may therefore be a slightly more enriched source or a lower degree of partial melting. Generally speaking, minor crustal contamination can result in negative Nb-Ta anomalies but also positive Zr-Hf anomalies due to the enrichment of these elements in crustal materials. The studied samples show negative Nb-Ta and positive Zr-Hf anomalies, suggesting that crustal contamination was not significant (Green, 2006). The relatively high Zr/Sm ratios (6.50 - 57.65) in these samples reflect the presence of a residual mineral that produces Zr (such as zircon). These high (Zr/Sm) ratios may be the result of crustal contamination because the upper

crust generally has high Zr/Sm ratios (32). Moreover, the absolute concentrations of incompatible elements (Nb, Ta, Zr, Sm, etc.) are much higher than those usually observed in crustal rocks [63]. In addition, the Ba (44.5 - 957.6 ppm) and Sr (7.1 - 786.6 ppm) of some rocks are much higher than those of the continental crust (Ba = 259 ppm; Sr = 348 ppm; Rudnick and Gao, 2003). Indeed, the continental crust exhibits relatively high Th/Ce ratios (0.15) and negative Eu anomalies [63], whereas mantle-derived magmas exhibit low Th/Ce ratios (0.013 - 0.05) [36] in pink granites but high in pink microgranites, syenites and granodiorites (0.14 - 0.56).

6.5. Geodynamic Context of Granitoid Emplacement

The geodynamic evolution of the Fianga Massif begins with the emplacement of quartz chlorite schists and massive amphibolites during the opening of the ocean around 770 Ma [3]. The granitoids of the outcropping massif are in the form of plutons of varying sizes intruding into the metamorphic rocks. These granitoids contain enclaves of quartz chlorite schists and massive oriented amphibolites. Petrography shows the micro-grained to coarse-grained texture of the granitoids. The plutonic intrusions represent the last magmatic manifestations associated with the Pan-African orogeny at the scale of the Fianga Massif.

The triangular diagram of Harris [65] (**Figure 12(a)**) shows that the pink

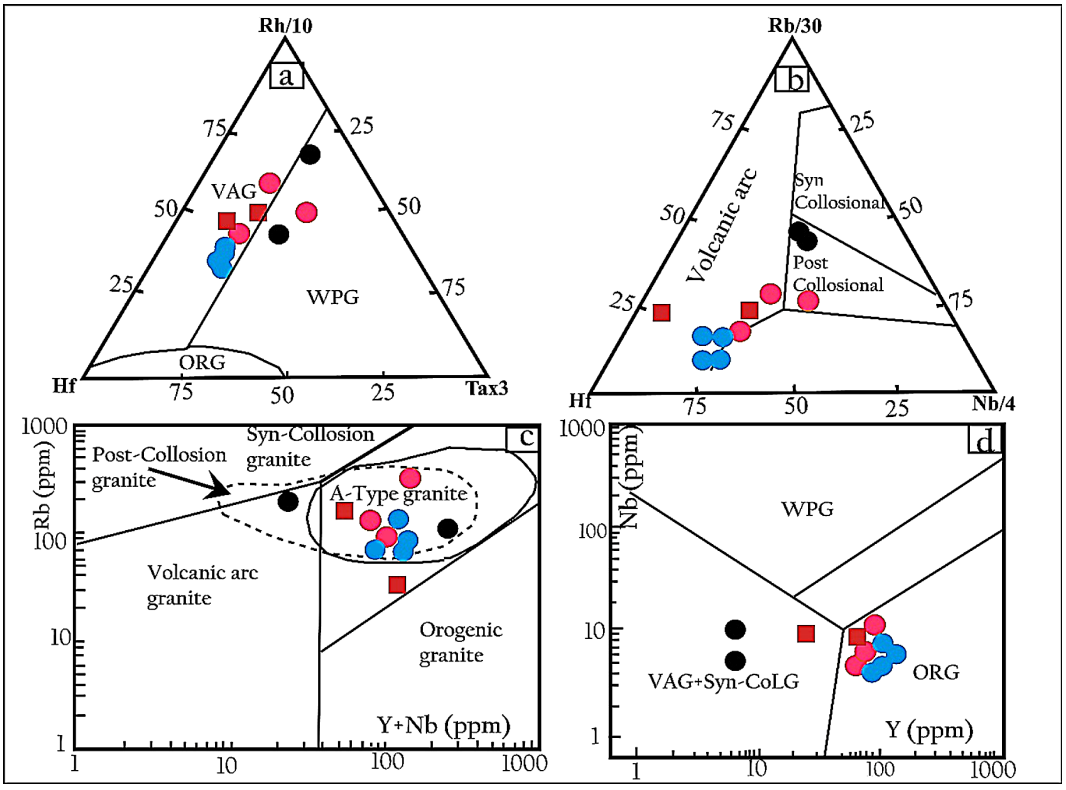

Figure 12. Position of franitoids of Fiangain the discrimination diagram ofthe geotectonic setting: (a) Hf-Rb/30-Ta*3, (b) Hf-Nb/4-Rb/30, (c) Rb vs (Y + Nb) discrimination diagram for the Fianga granitoids after Pearce *et al.* [64] and (d) Nb vs. Y [64].

granites, granodiorites and two pink microgranite samples fall within the domain of volcanic arc granitoids, except for the syenites and one pink microgranite sample which fall within the intraplate anorogenic domain. In the Hf-Nb/4-Rb/30 ternary diagram (**Figure 12(b)**), the pink granites, granodiorites and two pink microgranite samples fall within the domain of volcanic arc granitoids while the syenites and one pink microgranite sample fall within the intraplate anorogenic domain. In the Rb vs (Y + Nb) discrimination diagram ([64]; **Figure 12(c)**), all the studied rocks are clearly located in the field of syn-collisional granites except for one syenite sample and one granodiorite sample which belong respectively to the syn-collisional granitic field and to the intraplate anorogenic domain (WPG). These features and their potassium-rich calc-alkaline compositions are consistent with a continental collision context [13] [66]. Therefore, some intra-plate granitic features observed in most of the studied rocks (**Figure 12(c)**) can be interpreted as an evolutionary trend of the calc-alkaline suites. The Nb vs. Yb discriminant diagram [65] shows that pink granites and pink microgranites are located in the Oceanic Ripple Granitoids (ORG) domain and that syenites and granodiorites belong to the syn-collisional granitoids (Syn-COLG) domain (**Figure 12(d)**).

Multi-element diagrams (**Figure 13**) provide more information on the granitoid formation process, and in particular on the composition of the mantle source.

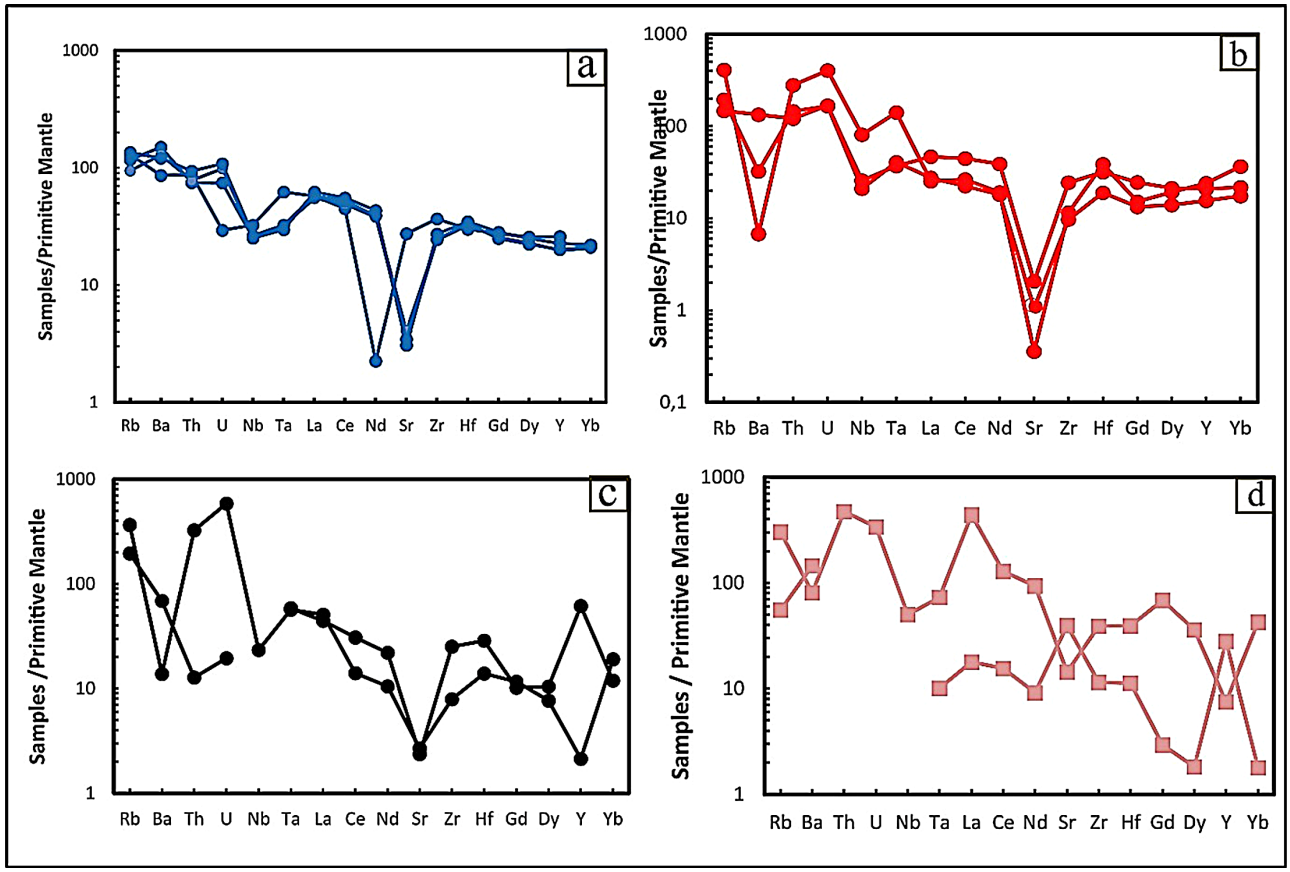

Figure 13. Multi-element diagrams of the Fianga granitoids normalized to the primitive [36]: (a) Pink granites, (b) pink microgranites, (c) Syenites and (d) Granodiorites.

Granodiorites show positive and negative anomalies in lithophile elements (LILE: Ba, Rb, Sr) and abnormally high contents of highly incompatible strong field effect elements (HFSE) (Th, U, LREE). The enrichment in these mobile elements can be explained by the input of water into the magma source during subduction. Indeed, the subducting plate contains water in the argillaceous pelagic sediment film and in the magmatic oceanic crust altered by seawater (ridge hydrothermalism). This water contained in the subduction rocks will be released when the plate reaches high depths and temperatures. The water from this plate will be transferred to the mantle wedge source of arc magmas and the mobile elements contained in the plate will follow the same path.

Immobile incompatible elements (Th, REE) may also be added to the magma source because when the temperature exceeds 600˚C in the submerging slab, pelagic sediments can melt.

The major characteristic of these magmas is their negative anomaly in Nb-Ta, two strong field effect elements (HFSE), highly incompatible and highly immobile (**Figure 13**). Several explanations can explain these anomalies:

- Nb and Ta are present at very low concentrations in the pelagic sediments; their contents are equivalent to those of MORBs. During dehydration of the submerging slab, due to their low content in the depleted mantle and their highly immobile behavior, there will be no enrichment in Nb-Ta in the mantle wedge source of the granitoids (**Figure 13**).

- Nb and Ta are highly incompatible elements, except in certain titaniferous minerals including rutile. During dehydration and melting of the sedimentary film covering the plunging plate, these elements will remain trapped in the dehydration or melting residue in the rutile (a refractory mineral that only melts at very high temperatures). The mantle wedge will therefore not be enriched in Nb-Ta compared to other mobile and incompatible elements (**Figure 13**).

In the Mayo-Kebbi domain, two types of post-collisional granitoids are known: calc-alkaline potassic [25] and alkaline [27]. The alkaline type formed following extreme fractional crystallization of a magma of mantle origin contaminated by a pre-Neoproterozoic source, while the calc-alkaline type results from partial melting of the lower crust. The Fianga granitoids are thought to have been emplaced in metasedimentary and metavolcanic formations around 570 Ma (U/Pb zircon, [25] [27]. These granitoids have geochemical and mineralogical similarities with the granitoids described as late post-tectonic or post-collisional, which only outcrop in the Adamawa-Yadé and North-West Cameroon domains [12] [13] [26] [24] in the Cameroonian portion of the Pan-African chain. Composed of granites, diorites, gabbros and syenites, they are predominantly very potassic calc-alkaline.

7. Conclusion

The Fianga area consists of plutonic formations intruding into metamorphic (amphibolite) formations: 1) pink granites, 2) pink microgranites, 3) syenites, and 4) granodiorites. Whole-rock geochemistry reveals an alkaline to transalkaline affin-

ity and a strong potassic affinity for the rocks of the study area. Combined field, petrographic, and geochemical data from the Fianga pluton suggest that these rocks originate from a single magmatic source and are differentiated by fractional crystallization in a deep magma chamber. The chemical composition of the medium-grained syenite suggests that the parental magma originated from partial melting of a metasomatized source in the lithospheric mantle. Major elements and rare earth elements indicate that the source of the Fianga magma was located near the base of the garnet-bearing herzolite peridotite mantle, in the lithospheric mantle. Petrographic relationships allow us to conclude that these plutonic formations were formed by a process of magmatic differentiation, notably fractional crystallization. All the facies studied, ranging from pink granite terms to granodiorite terms via syenite facies, form a transitional suite, characterized by moderate TiO_2 and P_2O_5 contents, and slightly enriched spectra of incompatible elements. For the Fianga magmatism, a process of fractional crystallization of a transitional felsic magma, which would produce the felsic series, coupled with an assimilation of continental crust, which would occur mainly at a late stage of magmatic differentiation, can be considered. This process would be responsible for the observed chemical peculiarities, namely the slight negative anomalies in Nb and the increase in certain ratios between incompatible elements, such as the Zr/Yb ratio in granitoids. The interaction of contaminated magmas with intermediate liquids would be at the origin of the heterogeneous facies and immiscibility figures.

Acknowledgements

This article is part of the first author's postdoctoral research. We would like to thank the anonymous reviewers and the associate editor for their critical review of the manuscript and their suggestions for substantial improvements.

Conflicts of Interest

The authors declare that they have no known competing financial interests or personal relationships that could have appeared to influence the work reported in this paper.

References

[1] Bessoles, B. and Trompette, M. (1980) Géologie de l'Afrique: La chaîne panafricaine, "zone mobile d'Afrique Central (partie sud) et zone mobile soudanaise". *Mémoire du Bureau de Recherche Géologiques et Minières*, **92**, Article 396.

[2] Oliveira, E.P., Toteu, S.F., Araújo, M.N.C., Carvalho, M.J., Nascimento, R.S., Bueno, J.F., *et al.* (2006) Geologic Correlation between the Neoproterozoic Sergipano Belt (NE Brazil) and the Yaoundé Belt (Cameroon, Africa). *Journal of African Earth Sciences*, **44**, 470-478. https://doi.org/10.1016/j.jafrearsci.2005.11.014

[3] Doumnang, J.C. (2006) La géologie des formations néoprotérozoïques du Mayo Kebbi (S-W du Tchad). Thèse de Doctorat, Orleans University.

[4] Isseini, M. (2011) Croissance et différenciation crustales au Néoprotérozoïque: Exemple du domaine panafricain du Mayo-Kebbi au Sud-Ouest du Tchad. Thèse de

Doctorat Université Henri Poincaré, 339 p.

[5] Mbaguedjé, D. (2015) Métallogénie de l'or et de l'uranium dans le cadre de la croissance et de la différenciation de la croûte au Néoprotérozoïque: Exemple du massif du Mayo-Kebbi (Tchad) dans la Ceinture Orogénique d'Afrique Centrale. Thèse de Doctorat en Géosciences. Université de Lorraine. 269 p.

[6] Djerossem, N.F. (2018) Croissance et remobilisation crustales au Pan-Africain dans le Sud du massif du Ouaddaï (Tchad oriental). Thèse de Doctorat en Géosciences Environnement Toulouse. Université Toulouse-3 Paul Sabatier. 302 p.

[7] Vanderhaeghe, O. (2009) Migmatites, Granites and Orogeny: Flow Modes of Partially-Molten Rocks and Magmas Associated with Melt/Solid Segregation in Orogenic Belts. *Tectonophysics*, **477**, 119-134. https://doi.org/10.1016/j.tecto.2009.06.021

[8] Brown, M. (2013) Granite: From Genesis to Emplacement. *Geological Society of America Bulletin*, **125**, 1079-1113. https://doi.org/10.1130/b30877.1

[9] Abdelsalam, M.G., Gao, S.S. and Liégeois, J.P. (2011) Upper Mantle Structure of the Saharan Metacraton. *Journal of African Earth Sciences*, **60**, 328-336. https://doi.org/10.1016/j.jafrearsci.2011.03.009

[10] Poidevin, J.L. (1991) Les ceintures de roches vertes de la République Centrafricaine. Contribution à la connaissance du Précambrien du nord du craton du Congo. Doctorat d'Etat, Université Blaise Pascal, Clermont-Ferrand (France), 208 p.

[11] Rolin, P. (1995) La zone de décrochements panafricains des Oubanguides en République Centrafricaine. *Comptes Rendu de l'Académie des Sciences de Paris*, **320**, 63-69.

[12] Toteu, S.F., Van Schmus, W.R., Penaye, J. and Michard, A. (2001) New U-Pb and Sm-Nd Data from North-Central Cameroon and Its Bearing on the Pre-Pan African History of Central Africa. *Precambrian Research*, **108**, 45-73. https://doi.org/10.1016/s0301-9268(00)00149-2

[13] Toteu, S.F., Penaye, J. and Djomani, Y.P. (2004) Geodynamic Evolution of the Pan-African Belt in Central Africa with Special Reference to Cameroon. *Canadian Journal of Earth Sciences*, **41**, 73-85. https://doi.org/10.1139/e03-079

[14] Toteu, S.F., Penaye, J., Deloule, E., Van Schmus, W.R. and Tchameni, R. (2006) Diachronous Evolution of Volcano-Sedimentary Basins North of the Congo Craton: Insights from U-Pb Ion Microprobe Dating of Zircons from the Poli, Lom and Yaoundé Groups (Cameroon). *Journal of African Earth Sciences*, **44**, 428-442. https://doi.org/10.1016/j.jafrearsci.2005.11.011

[15] Ngako, V., Affaton, P., Nnange, J.M. and Njanko, T. (2003) Pan-African Tectonic Evolution in Central and Southern Cameroon: Transpression and Transtension during Sinistral Shear Movements. *Journal of African Earth Sciences*, **36**, 207-214. https://doi.org/10.1016/s0899-5362(03)00023-x

[16] Wacrenier, P. (1953) Notice provisoire de la carte géologique de Moundou Ouest. Rapport T12 de fin de mission, 1953. Direction de mines. A.E.F., Brazzaville, 18 p.

[17] Wacrenier, P. (1962) Carte géologique de reconnaissance des Etats d'Afrique Equatoriale, feuille NC 33 SO E-53 SE O-54 (Moundou) 1/500 000. IRGM. Brazzaville.

[18] Kasser, M.Y. (1995) Evolution Précambrienne de la région du Mayo-Kebbi (S-W du Tchad), un segment de la chaîne Panafricaine. Thèse Muséum National d'Histoire Naturelle de Paris, 217 p.

[19] Klamadji, M.N., Dedzo, M.G., Tchameni, R., Hamadjoda, D.D., Nyotok, P.C.B.À. and Onana, G. (2021) Fractional Crystallization and Crustal Contamination of Doleritic and Trachytic Dykes Crosscutting the Cretaceous Sedimentary Basins from Figuil

(North Cameroon) and Léré (South-Western Chad): Geodynamic Implications. *Journal of Geoscience and Environment Protection*, **9**, 190-210. https://doi.org/10.4236/gep.2021.912012

[20] Affaton, P., Rahaman, M.A., Trompette, R. and Sougy, J. (1991) The Dahomeyide Orogen: Tectono-Thermal Evolution and Relationships with the Volta Basin. In: Dallmeyer, R.D. and Lecorche, J.P.C.L., *The West African Orogens and Circum-Atlantic Correlatives*, Springer, 107-122.

[21] Louis, P. (1970) Contribution géophysique à la connaissance géologique du bassin du lac Tchad.

[22] Penaye, J., Kröner, A., Toteu, S.F., Van Schmus, W.R. and Doumnang, J. (2006) Evolution of the Mayo Kebbi Region as Revealed by Zircon Dating: An Early (ca. 740Ma) Pan-African Magmatic Arc in Southwestern Chad. *Journal of African Earth Sciences*, **44**, 530-542. https://doi.org/10.1016/j.jafrearsci.2005.11.018

[23] Kusnir, I. and Moutaye, H.A. (1997) Ressources minérales du Tchad: une revue. *Journal of African Earth Sciences*, **24**, 549-562. https://doi.org/10.1016/s0899-5362(97)00080-8

[24] van Schmus, W.R., Oliveira, E.P., da Silva Filho, A.F., Toteu, S.F., Penaye, J. and Guimarães, I.P. (2008) Proterozoic Links between the Borborema Province, NE Brazil, and the Central African Fold Belt. *Geological Society, London, Special Publications*, **294**, 69-99. https://doi.org/10.1144/sp294.5

[25] Pouclet, A., Vidal, M., Doumnang, J.C., Vicat, J.P. and Tchameni, R. (2006) Neoproterozoic Crustal Evolution in Southern Chad: Pan-African Ocean Basin Closing, Arc Accretion and Late- to Post-Orogenic Granitic Intrusion. *Journal of African Earth Sciences*, **44**, 543-560. https://doi.org/10.1016/j.jafrearsci.2005.11.019

[26] Ngako, V., Affaton, P. and Njonfang, E. (2008) Pan-African Tectonics in Northwestern Cameroon: Implication for the History of Western Gondwana. *Gondwana Research*, **14**, 509-522. https://doi.org/10.1016/j.gr.2008.02.002

[27] Isseini, M., André-Mayer, A., Vanderhaeghe, O., Barbey, P. and Deloule, E. (2012) A-Type Granites from the Pan-African Orogenic Belt in South-Western Chad Constrained Using Geochemistry, Sr-Nd Isotopes and U-Pb Geochronology. *Lithos*, **153**, 39-52. https://doi.org/10.1016/j.lithos.2012.07.014

[28] Schwoerer, P. (1965) Carte géologique de reconnaissance à l'échelle du 1/500 000 et Notice explicative sur la feuille Garoua-Est, Dir.

[29] Le Bas, M., Le Maitre, S.A. and Zanettin, B. (1986) A Chemical Classification of Volcanic Rocks Based on the Total Alkali-Silica Diagram. *Journal of Petrology*, **27**, 745-750. https://doi.org/10.1093/petrology/27.3.745

[30] Maniar, P.D. and Piccoli, P.M. (1989) Tectonic Discrimination of Granitoids. *Geological Society of America Bulletin*, **101**, 635-643. https://doi.org/10.1130/0016-7606(1989)101<0635:tdog>2.3.co;2

[31] Peccerillo, A. and Taylor, S.R. (1976) Geochemistry of Eocene Calc-Alkaline Volcanic Rocks from the Kastamonu Area, Northern Turkey. *Contributions to Mineralogy and Petrology*, **58**, 63-81. https://doi.org/10.1007/bf00384745

[32] White, J.R. and Chappell, B.W. (1977) Ultrametamorphism and Granitoids Genesis. Ultrametamorphism and Granitoid Genesis. *Tectonophysics*, **43**, 7-22. https://doi.org/10.1016/0040-1951(77)90003-8

[33] Zen, E. (1986) Aluminum Enrichment in Silicate Melts by Fractional Crystallization: Some Mineralogic and Petrographic Constraints. *Journal of Petrology*, **27**, 1095-1117. https://doi.org/10.1093/petrology/27.5.1095

[34] Morrison, G.W. (1980) Characteristics and Tectonic Setting of the Shoshonite Rock Association. *Lithos*, **13**, 97-108. https://doi.org/10.1016/0024-4937(80)90067-5

[35] Müller, D., Rock, N.M.S. and Groves, D.I. (1992) Geochemical Discrimination between Shoshonitic and Potassic Volcanic Rocks in Different Tectonic Settings: A Pilot Study. *Mineralogy and Petrology*, **46**, 259-289. https://doi.org/10.1007/bf01173568

[36] McDonough, W.F. and Sun, S.S. (1995) The Composition of the Earth. *Chemical Geology*, **120**, 223-253. https://doi.org/10.1016/0009-2541(94)00140-4

[37] Green, N.L. (2006) Influence of Slab Thermal Structure on Basalt Source Regions and Melting Conditions: REE and HFSE Constraints from the Garibaldi Volcanic Belt, Northern Cascadia Subduction System. *Lithos*, **87**, 23-49. https://doi.org/10.1016/j.lithos.2005.05.003

[38] Didier, J. (1973) Granites and Their Enclaves: The Bearing of Enclaves on the Origin of Granites. Elsevier.

[39] Barbarin, B. and Didier, J. (1992) Genesis and Evolution of Mafic Microgranular Enclaves through Various Types of Interaction between Coexisting Felsic and Mafic Magmas. *Earth and Environmental Science Transactions of the Royal Society of Edinburgh*, **83**, 145-153. https://doi.org/10.1017/s0263593300007835

[40] Barbarin, B. (1989) Importance des différents processus d'hybridation dans les plutons granitiques du batholite de la Sierra Nevada, Californie. Schweiz. *Mineralogy and Petrogrology Mitterrand*, **69**, 303-315.

[41] Roberts, M.P. and Clemens, J.D. (1993) Origin of High-Potassium, Talc-Alkaline, I-Type Granitoids. *Geology*, **21**, 825-828. https://doi.org/10.1130/0091-7613(1993)021<0825:oohpta>2.3.co;2

[42] Poli, G.E. and Tommasini, S. (1999) Geochemical Modeling of Acid-Basic Magma Interaction in the Sardinia-Corsica Batholith: The Case Study of Sarrabus, Southeastern Sardinia, Italy. *Lithos*, **46**, 553-571. https://doi.org/10.1016/s0024-4937(98)00082-6

[43] Roberts, M.P., Pin, C., Clemens, J.D. and Paquette, J. (2000) Petrogenesis of Mafic to Felsic Plutonic Rock Associations: The Calc-Alkaline Quérigut Complex, French Pyrenees. *Journal of Petrology*, **41**, 809-844. https://doi.org/10.1093/petrology/41.6.809

[44] Foley, S.F., Venturelli, G., Green, D.H. and Toscani, L. (1987) The Ultrapotassic Rocks: Characteristics, Classification, and Constraints for Petrogenetic Models. *Earth-Science Reviews*, **24**, 81-134. https://doi.org/10.1016/0012-8252(87)90001-8

[45] Grove, T.L. and Kinzler, R.J. (1986) Petrogenesis of Andesites. *Annual Review of Earth and Planetary Sciences*, **14**, 417-454. https://doi.org/10.1146/annurev.ea.14.050186.002221

[46] Barbarin, B. (1999) A Review of the Relationships between Granitoid Types, Their Origins and Their Geodynamic Environments. *Lithos*, **46**, 605-626. https://doi.org/10.1016/s0024-4937(98)00085-1

[47] Thompson, R.N. and Morrison, M.A. (1988) Asthenospheric and Lower-Lithospheric Mantle Contributions to Continental Extensional Magmatism: An Example from the British Tertiary Province. *Chemical Geology*, **68**, 1-15. https://doi.org/10.1016/0009-2541(88)90082-4

[48] Saunders, A.D., Storey, M., Kent, R.W. and Norry, M.J. (1992) Co, Sequences of Plume Lithosphere Interactions. Magmatism and the Cause of Continental Breakup. *Geological Society of London*, *Special Publication*, **68**, 41-60.

[49] Frey, F.A., Green, D.H. and Roy, S.D. (1978) Integrated Models of Basalt Petrogenesis: A Study of Quartz Tholeiites to Olivine Melilitites from South Eastern Australia

Utilizing Geochemical and Experimental Petrological Data. *Journal of Petrology*, **19**, 463-513. https://doi.org/10.1093/petrology/19.3.463

[50] Klamadji, M.N., Dedzo, M.G., Tchameni, R. and Dawaï, D. (2020) Petrography and Geochemical Characterization of Dolerites from Figuil (Northern Cameroon) and Léré (Southwestern Chad). *International Journal of Geosciences*, **11**, 459-482. https://doi.org/10.4236/ijg.2020.117023

[51] Ngarena, K.M., Léotine, T., Gustave, B.R., Dedzo, M.G., Felix, D.N., Felix, B.L., *et al.* (2025) Geochemical Characterizations of the Hypovolcanic Formations of the Pan-African Basement and the Cretaceous Sedimentary Basins of Figuil (North Cameroon) and Léré (South-West Chad): Petrogenetic and Geodynamic Implication of the Pan-African Range of Central Africa (CPAC). *International Journal of Geosciences*, **16**, 127-153. https://doi.org/10.4236/ijg.2025.162007

[52] DePaolo, D.J. (1981) Trace Element and Isotopic Effects of Combined Wall Rock Assimilation and Fractional Crystallisation. *Earth and Planetary Science Letters*, **84**, 59-68.

[53] Condie, K.C. (1997) Sources of Proterozoic Mafic Dyke Swarms: Constraints from Th/Ta and La/Yb Ratios. *Precambrian Research*, **81**, 3-14. https://doi.org/10.1016/s0301-9268(96)00020-4

[54] Siégel, C., Bryan, S.E., Allen, C.M. and Gust, D.A. (2018) Use and Abuse of Zircon-Based Thermometers: A Critical Review and a Recommended Approach to Identify Antecrystic Zircons. *Earth-Science Reviews*, **176**, 87-116. https://doi.org/10.1016/j.earscirev.2017.08.011

[55] Tchameni, R., Pouclet, A., Penaye, J., Ganwa, A.A. and Toteu, S.F. (2006) Petrography and Geochemistry of the Ngaoundéré Pan-African Granitoids in Central North Cameroon: Implications for Their Sources and Geological Setting. *Journal of African Earth Sciences*, **44**, 511-529. https://doi.org/10.1016/j.jafrearsci.2005.11.017

[56] Liankun, S. and Kuirong, Y. (1989) A Tow-Stage Crust-Mantel Interaction Model for Mafic Microgranular Enclaves in the Daning Granodiorite Pluton, Guangxi, China. In: Didier, J. and Barbarin, B., *Enclaves and Granite Petrology*, *Development of Petrology*, Elsevier, 95-110.

[57] Le Maître, R.W. (2002) Igneous Rocks. A Classification and Glossary of Terms. Recommendations of the International Union of Geological Sciences Sub Commission on the Systematics of Igneous Rocks, Cambridge. Cambridge University Press.

[58] McKenzie, D. and O'Nions, R.K. (1991) Partial Melt Distributions from Inversion of Rare Earth Element Concentrations. *Journal of Petrology*, **32**, 1021-1091. https://doi.org/10.1093/petrology/32.5.1021

[59] Pearce, J.A. and Peate, D.W. (1995) Tectonic Implications of the Composition of Volcanic Arc Magmas. *Annual Review of Earth and Planetary Sciences*, **23**, 251-285. https://doi.org/10.1146/annurev.earth.23.1.251

[60] Grove, T.L., Parman, S.W., Bowring, S.A., Price, R.C. and Baker, M.B. (2002) The Role of an H_2O-Rich Fluid Component in the Generation of Primitive Basaltic Andesites and Andesites form the Mt Shasta Region, N. California. *Contributions to Mineralogy and Petrology*, **142**, 375-396. https://doi.org/10.1007/s004100100299

[61] Sun, S.S. and McDonough, W.F. (1989) Chemical and Isotopic Systematics of Oceanic Basalts: Implication for Mantle Composition and Processes. In: Saundersand, A.D. and Norry, M.J., *Magmatism in the Ocean Basins*, Geological Society Special Publication, 313-345.

[62] Aldanmaz, E., Pearce, J.A., Thirlwall, M.F. and Mitchell, J.G. (2000) Petrogenetic Evolution of Late Cenozoic, Post-Collision Volcanism in Western Anatolia, Turkey.

Journal of Volcanology and Geothermal Research, **102**, 67-95. https://doi.org/10.1016/s0377-0273(00)00182-7

[63] Taylor, S.R. and McLennan, S.M. (1995) The Geochemical Evolution of the Continental Crust. *Reviews of Geophysics*, **33**, 241-265. https://doi.org/10.1029/95rg00262

[64] Pearce, J.A., Harris, N.B.W. and Tindle, A.G. (1984) Trace Element Discrimination Diagrams for the Tectonic Interpretation of Granitic Rocks. *Journal of Petrology*, **25**, 956-983. https://doi.org/10.1093/petrology/25.4.956

[65] Harris, N.B.W., Pearce, J.A. and Tindle, A.G. (1986) Geochimical Characteristics of Collision-Zone Magmatism. In: Coward, M.P. and Reis, A.C., *Collision Tectonics*, Geological Society, Special Publications, 67-81.

[66] Liégeois, J.P., Black, R., Navez, J. and Latouche, L. (1994) Early and Late Pan-African Orogenies in the Aïr Assembly of Terranes (Tuareg Shield, Niger). *Precambrian Research*, **67**, 59-88. https://doi.org/10.1016/0301-9268(94)90005-1